8 Resistive plate chambers

In the barrel region, trigger signals are provided by a system of Resistive Plate Chambers (RPCs). Given the high background rates at the LHC (Chapter 2,[8-1]), the muon drift chambers will have to operate at high levels of occupancy. For this reason, it was decided to use an independent, dedicated, fast and hence low-occupancy chamber system for trigger purposes.

The main tasks required of the ATLAS trigger system are:

- coarse measurement of and discrimination on the muon transverse momentum p_T;
- bunch crossing identification;
- fast and coarse tracking to identify the hits of the precision chambers that are related to the detected muon track;
- 2nd-coordinate measurement with a required resolution of 5–10 mm.

The trigger detector in the barrel is made up of three stations each with two detector layers. Two stations installed at a distance of 50 cm from each other are located near the centre of the magnetic field region and provide the low-p_T trigger ($p_T > 6$ GeV) while the third station, at the outer radius of the magnet, allows to increase the p_T threshold to 20 GeV, thus providing the high-p_T trigger. The trigger logic requires three out of four layers in the middle stations for the low p_T trigger and, in addition, one of the two outer layers for the high-p_T trigger.

8.1 Operating principles and typical performance

The RPC is a gaseous parallel-plate detector with a typical space–time resolution of the order of 1 cm $\times$ 1 ns with digital readout. This resolution is well suited to fulfill the requirements of the ATLAS trigger system.

RPCs do not use wires and are simple to manufacture. Two resistive plates, made of Bakelite, are kept parallel to one another by insulating spacers, which define the size of the gas gap. A uniform electric field of a few kV/mm produces the avalanche multiplication of the ionization electrons. The signal is read out via capacitative coupling to metal strips placed at both sides of the detector and grounded virtually. The RPC design is described in detail in Section 8.2.

RPCs can be operated both in avalanche [8-2] and streamer mode. In a high background environment, as in the case of the LHC, the avalanche mode operation offers higher rate capability and stable timing performance independent of the counting rate. This is due to the much smaller charge delivered in the gas by an avalanche with respect to a streamer.

The avalanche-mode operation requires a high signal amplification in the front-end electronics to compensate for the low gas amplification. The front-end electronics is described in Section 8.4.

For avalanche operation we have identified a new non-flammable, environmentally safe gas, tetrafluoroethane ($C_2H_2F_4$). This gas is characterized by high density, relatively low operating voltage, low cost and easy availability, typical for a widely used industrial product. Other gases are under study.

Several gas mixtures have been tested for avalanche-mode operation containing relatively modest amounts of argon and / or butane added to the tetrafluoroethane. The binary mixture $C_2H_2F_4$ / iso-C_4H_{10} has been extensively studied both in beam and cosmic ray tests. It has a flammability threshold of 5.75% butane. This limit implies no major problems since the detector performance has been found to be only weakly dependent on the amount of C_4H_{10} in the range from 10% down to 1.6%. The baseline gas is $C_2H_2F_4$ / iso-C_4H_{10} in the mixing ratio 97%/3%.

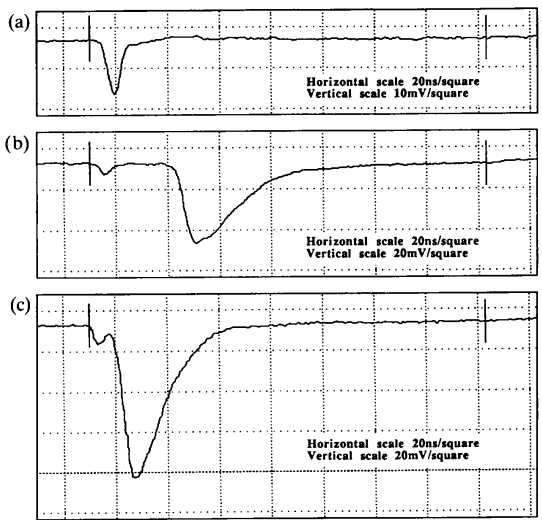

Figure 8-1 Signal waveforms induced by cosmic rays at different operating voltages. The avalanche signal at 9.4 kV has a typical duration of about 5 ns FWHM (a). In (b), at 9.6 kV, the avalanche signal is followed by a streamer. The avalanche-to-streamer delay becomes gradually shorter at higher voltages ((c), 10.2 kV). The gas mixture: is$C_2H_2F_4$/*n*-C_4H_{10}/Ar (83%/7%/10%.

The avalanche signal in RPCs (Figure 8-1 (a)), exhibits a single peak with a rise time of about 2 ns and a FWHM of 5 ns, both depending on the gas mixture [8-3]. This waveform is detected directly on the pick-up strip and no front-end electronics was used. Nevertheless the quoted times may be affected by the scope bandwidth (400 MHz) and the long BNC cable (80 ns) used to send the strip signal into the scope, so they must be taken as upper limits. This well-defined time structure is quite different from the one of a wire chamber signal that, if observed with sufficient frequency bandwidth, appears as a series of peaks due to the primary clusters arriving in sequence at the multiplication region near the wire [8-4]. In the uniform field of an RPC, all the clusters give rise to simultaneous avalanches that produce a single signal with very low time jitter. The charge multiplication in each avalanche continues until the avalanche arrives at the anode plane where it is absorbed and removed from the gas. The gas gain of each cluster, $G \sim \exp(\alpha d_i)$, α being the first Townsend coefficient, depends on the distance d_i of the primary cluster from the anode plane. The signal charge is therefore dominated by a few clusters produced at the largest distances from the anode plane. As a consequence the charge distribution in RPCs is wider than in wire detectors where all the primary clusters have approximately the same gain.

The transition from avalanche-mode to streamer-mode operation can be inferred from the study of the signal waveform. If the operating voltage is increased above a threshold that depends on the gas, the RPC avalanche signal described above may be followed by a much larger signal (Figure 8-1 (b), (c)) due to the growth of a streamer. The streamer probability increases with the operating voltage. This is further discussed in Section 8.5.

The avalanche delay is weakly dependent on the operating voltage. The linear fit to the experimental data has a slope of (-4.5 ± 0.2) ns / kV (Figure 8-2). The streamer delay with respect to the avalanche precursor has a more complex dependence on the voltage. The linear fit of the data, shown in Figure 8-3, has a very similar slope, (-4.4 ± 0.2) ns / kV, above 10 kV where the streamer probability approaches unity. At lower voltages, i.e. in the range of the transition from avalanche to streamer, the delay can change by up to 20 ns for a voltage difference of only 100 V. The timing in avalanche mode is therefore more stable with respect to changes in the operating voltage. This means also stability with respect to the counting rate because a high rate produces

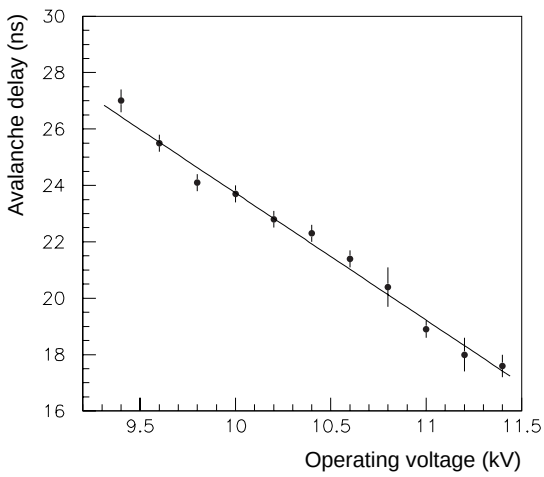

Figure 8-2 Avalanche delay with respect to the triggering signal, as a function of operating voltage

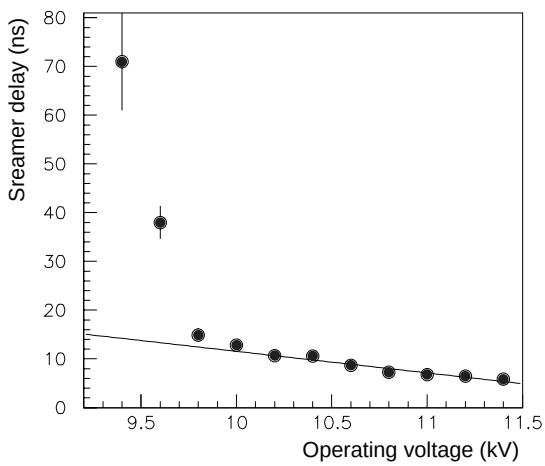

Figure 8-3 Streamer delay with respect to the avalanche precursor, as a function of operating voltage

a large total current flowing through the resistive electrodes that can reduce the voltage applied to the gas.

The long avalanche-to-streamer delay observed just above the streamer threshold indicates that the streamer is not a direct evolution of the avalanche but rather a delayed stage in which, owing to subsequent gas photoionization processes, the discharge propagates, presumably from the anode to the cathode plane, until a thin plasma column connecting the two electrodes is created. Any further development of the discharge, e.g. from the streamer to the spark stage, is prevented by the high resistivity of the electrode plates which limits the energy available to the discharge.

The different operation modes for a given gas can be identified in the plot of the average signal charge vs. the operating voltage (Figure 8-4). The fast linear increase of log<Q> at low voltages, $(1/Q)(dQ/dV) = 0.5\%/V$, is also observed in the case of wire detectors [8-5] and is characteristic of the proportional mode. At higher voltages, avalanche saturation and subsequent streamer formation are observed. Above the streamer threshold the avalanche 'precursor' charge and the total charge, mostly due to the streamer, are plotted separately. The slope of the avalanche charge is much lower than before,

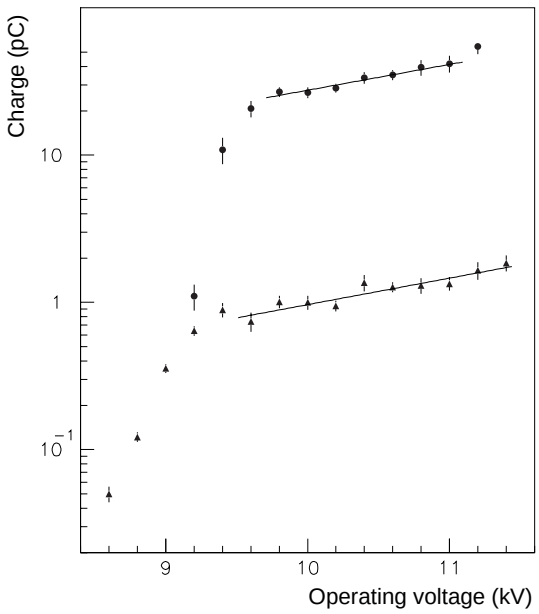

Figure 8-4 Average signal charge vs. operating voltage. Above the streamer threshold, the avalanche precursor charge (triangles) and the total charge (circles) are represented. The gas mixture is the same as in Figure 8-1.

$(1/Q)(dQ/dV) = 0.04\%/V$, showing a clear saturation effect. The streamer-to-avalanche charge ratio, about 40, is almost voltage independent.

The saturation of the avalanche is also documented by the change of the charge distribution shape vs. the operating voltage below the streamer threshold. In the proportional mode the avalanche charge distributions show a typical shape with a sharp rise edge and a long exponential tail. As the voltage approaches the condition of saturated avalanche the distributions become more and more symmetrical around the peak.

RPC operation in avalanche mode provides good rate capability and stable timing performance. The streamer mode must be avoided because of the large time jitter of the streamer signal and the large charge, which will increase the operating current and will trigger a large number of discrimination thresholds, optimized for avalanche operation. Therefore the streamer probability must be kept as low as possible. Tests on prototypes show that a streamer probability lower than 1% is achievable (Section 8.5).

The relevant parameters of RPCs are summarized in Table 8-1. In particular, the rate capability was measured by irradiating RPCs with μ/π beams [8-6] and intense γ sources [8-7].

The γ sensitivity was measured using photons from a ^{60}Co source [8-7].

Table 8-1 Performance specifications of RPCs

Intrinsic detection efficiency (single layer)	> 98.5%
Efficiency including spacers and frames	> 97%
Intrinsic time jitter (within 3 σ)	< 5 ns
Time jitter including strip propagation time	< 10 ns
Rate capability	~ 1 kHz/cm^2
1 MeV photon sensitivity	1%
Streamer probability per muon signal	< 1%

8.2 Mechanical design and construction

8.2.1 Layout of the basic two-layer chamber

The mechanical structure of the ATLAS trigger chambers must satisfy the following requirements:

- low thickness to minimize multiple scattering;
- independent mechanical supports to avoid mechanical stresses on the precision chambers.

A trigger chamber is made of two rectangular detector layers. Each of them is read out by two orthogonal series of pick-up strips: the η strips parallel to the MDT wires provide the ‘bending coordinate’ of the trigger detector; the ϕ strips, orthogonal to the wires, provide the second coordinate. The trigger logic uses both η and ϕ strips.

The detector is made of two Bakelite plates 2 mm thick of volume resistivity $10^{10}\,\Omega$ cm which are kept parallel to one another by polycarbonate spacers of 12 mm diameter and (2.00 ± 0.01) mm thickness which define the size of the gas gap. The spacers are glued on both plates at a distance of 10 cm from one another. A 7 mm wide frame of the same material, thickness and tolerance as the spacers is used to seal the gas gap all around the edge. Four gas inlets/outlets of 3 mm internal diameter are fixed at the corners of the detector. All parts of the mechanical structure, i.e. the plates, the spacers, the frame and the gas inlets are bonded together using epoxy adhesives. The structure of an RPC is shown in the photograph of Figure 8-5.

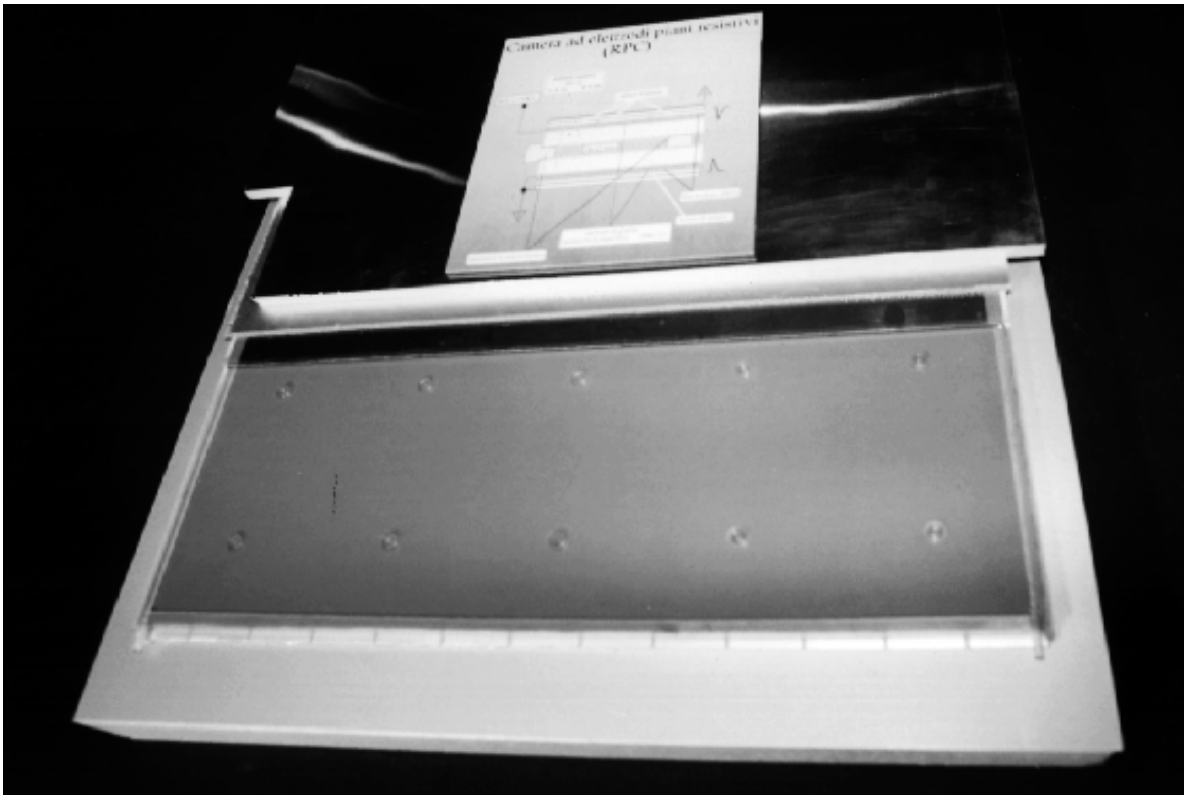

Figure 8-5 RPC structure. One of the plates has been cut to show the details of the inner chamber structure.

The outside surfaces of the resistive plates are coated with thin layers of graphite paint of a surface resistivity of about 100 kΩ which are connected to the high-voltage supply. These graphite electrodes are insulated with respect to the pick-up strips by means of 200 μm thick Polyethylene-Teraphtalate (PET) films which are glued on both graphite layers. The described mechanical structure will be referred to as ‘gas volume’.

The maximum dimensions of the gas volume are limited by the size of the Bakelite plates commercially available. In particular, the length of a gas volume cannot exceed 3.2 m. Therefore, in the BML and BOL chambers which exceed this limit, each detector layer is made of two identical gas volumes lined up in the direction of the longer side with the gas inlets interconnected in the middle of the detector. The dead zone remaining between the two gas volumes due to the edge sealing frames is 14 mm.

The readout strips are bonded over a plate of 3 mm thick expanded polystyrene which has an aluminium grounded reference sheet fixed on the opposite face. This ‘strip panel’ contains also the front-end electronics boards which are fixed along the edges as described in Section 8.4. The

ϕ strips cover the full width of the chamber up to a maximum of 108 cm. In the case of the η strips the full length of the chamber is covered by two identical strip panels which are read out by front-end electronics boards located at both ends of the chamber so that the strip is limited to a maximum length of 249 cm, and the corresponding propagation time is < 11 ns.

Each chamber is made of two detector layers and four readout strip panels. All these elements are superimposed and clamped together by means of two support panels which also provide the required stiffness to the chambers. The details of the chamber mechanical structure are shown in Figure 8-6. Each panel is made of an expanded polystyrene plate of density 40 kg / m^3 sandwiched between two aluminium sheets which are glued on it with epoxy adhesives. One of the two panels is flat, 50 mm thick, with 0.5 mm thick aluminium ‘skins’; the other panel is only 10 mm thick with 0.3 mm skins and is pre-bent with a sagitta of 5–10 mm, depending on the chamber width. The two panels are rigidly connected at the long sides by means of 2 mm thick aluminium profiles shaped as shown in Figure 8-6, so that the pre-bent support panel provides uniform pressure over the whole surface of the RPC module.

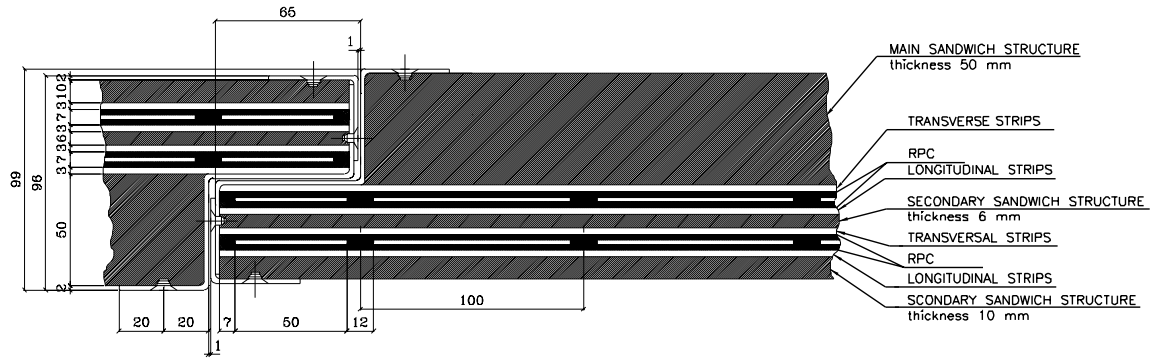

Figure 8-6 RPC trigger chamber cross section. The spacers and the sealing frames are shown inside the gas volume.

To avoid dead areas between contiguous chambers, the detector layers overlap in the z direction as shown in Figure 8-6. The thick support panels are narrower than the detector layers so as not to increase the overall thickness of the trigger chambers. The overlap is 60 mm and allows dead areas to be eliminated for particles with incident angles up to 40°. Clearance between chambers in the z direction is 10 mm and allows the interconnection of the front-end electronics and the local trigger electronics with flat cables as shown in Figure 8-7.

The trigger chambers are independently connected to the rails which support the muon detector in the barrel region. As in the case of the MDTs they are kinematically supported in three points (Figure 8-8).

Detailed Finite Element (FE) analysis calculations on the mechanical structure of the chambers have been carried out. The computed sagittae for the four main chamber sizes, BMS, BML, BOS, BOL assumed to be in horizontal position (case of maximum sagitta) are given in Table 8-2. The cases of fixed ends and supported ends are both shown in Table 8-2.The real case depends on the precise chamber connection to the rails; it is quite similar to the supported end case. The results given in the table show that the chamber mechanical structure has good stiffness. The resulting bending has no effect on the RPC performance.

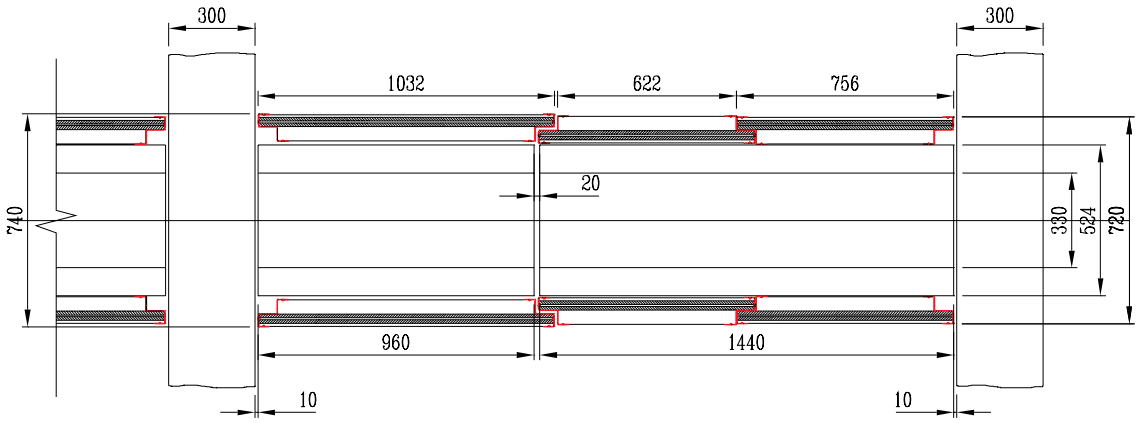

Figure 8-7 RPC chamber layout

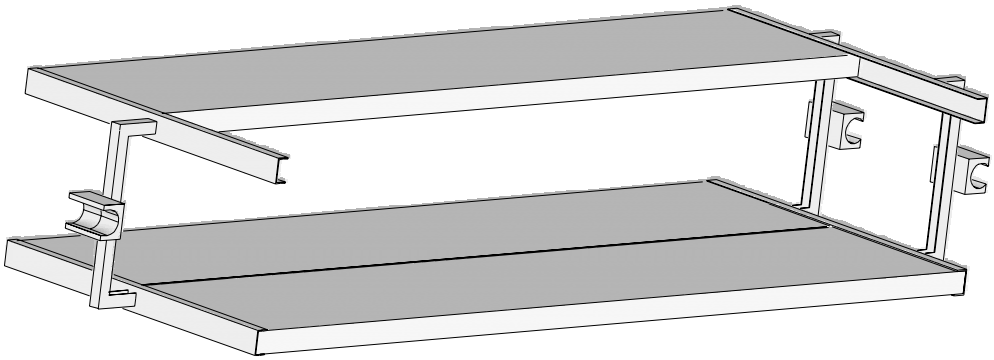

Figure 8-8 Trigger chamber connections to the support rails

Table 8-2 Computed gravitational sagittae of the trigger chambers, in a horizontal position (linear analysis)

Chamber type	Length (mm)	Width (mm)	Fixed end sagitta (mm)	Supported end sagitta (mm)
BMS	3300	748	0.46	1.85
BML	3700	748	0.73	2.8
BOS	3400	1080	0.53	2.0
BOL	5220	1080	2.3	10.8

The finite element calculations were verified with mechanical tests on full- and reduced-scale prototypes of the thick support plate. In both cases the panels were loaded to simulate the weight of the chambers. In the test condition the panel was the only element providing stiffness to the mechanical structure and the measured sagitta was therefore much larger than in the real case. The large-sized prototype [8-8] had phenolic honeycomb with 2 mm thick fibreglass skins. The reduced-size prototype had polystyrene foam of density 32 kg / m^3 with 0.5 mm thick aluminium skins. The latter solution was chosen for the lower weight and higher rigidity. Figure 8-9 shows the sagitta of the aluminium / polystyrene panel of size 1800×200 mm^2 supported at the ends and loaded with equal weights located at 1 / 4, 1 / 2 and 3 / 4 of the panel length. The results of the FE calculations are given for comparison.

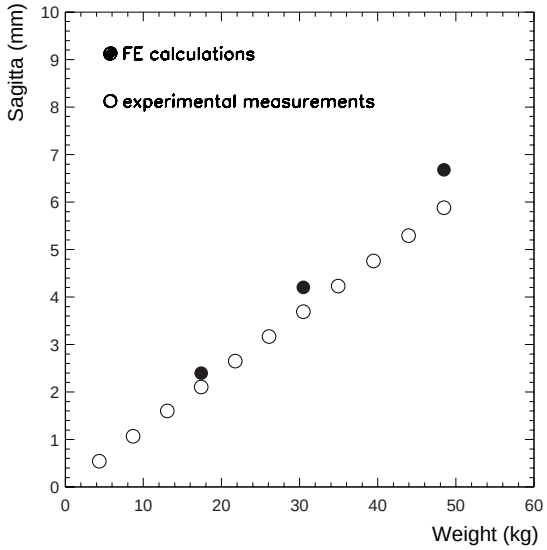

Figure 8-9 Measured sagitta of a test panel vs. weight. Also shown are predictions from finite element (FE) analysis calculations.

8.2.2 Assembly procedure

The construction programme comprises 596 chambers ranging from 0.96×3.1 m^2 to 2.2×5 m^2 in area (Chapter 4). They will cover the barrel middle layer twofold and the barrel outer layer onefold (Figure 4-25). The total area is $A_{tot} = 2 \times A_{middle} + A_{outer} = 3320$ m^2, corresponding to 6640 m^2 of single-gap gas volumes.

RPCs are industrially manufactured and their production procedure has been well established in the construction of the RPC systems which are used in the experiments L3 [8-9] and BaBar [8-10]. The presently existing facilities allow the production of 2200 m^2 of monogap RPCs for BaBar in less than one year.

Figure 8-10 The RPC graphite spraying facility

The production process is briefly described here. The Bakelite plates, of standard industrial production, are masked at the edges and then sprayed with graphite by means of an airless system using seven nozzles as shown in Figure 8-10. A small tin-coated copper electrode 50 µm thick which is needed to connect the graphite layer to the high-voltage supply is then glued at one corner of the plate with a conductive adhesive.

Figure 8-11 The PET film is glued on the graphite by means of a 'hot melt' facility

With the purpose of insulating the graphite layer from the pick-up electrodes a 200 µm thick PET film is subsequently glued on the graphite using 'hot melt' adhesives.

The facility developed for this purpose is shown in Figure 8-11. A 50 µm thick layer of hot liquid adhesive is deposited over the film which moves at a constant speed. A few seconds later the film is pressed against the plate by two rotating rubber cylinders so that the adhesive, still hot, bonds the film to the plate. The subsequent cooling at room temperature makes the adhesive solid and stable.

Two Bakelite plates prepared according to the described procedure are then coupled to each other by means of spacers and of a frame sealing the gas gap all around the edge. The frame and the spacers (both made of polycarbonate) are put in position by proper masks and glued to the plates with epoxy adhesives. During the glue curing the plates are pressed together with a vacuum system.

The spacers are produced by pressing the polycarbonate at high temperature. The frame is currently made from rectified polycarbonate plates. For the future, production by extrusion is envisaged.

After the gas volumes have been assembled, their internal surface is coated with a thin, uniform solid layer of linseed oil which defines the surface properties of the detector independently of the original electrode plate's surface and of the possible damage it could have suffered during the construction procedure. The gas volumes are kept in vertical position and then filled with a mixture of linseed oil and pentane used as solvent. They are subsequently emptied at low constant velocity and finally fluxed with clean dry air. The oxygen from the air triggers a polymerization reaction which makes the layer solid. The effect of this coating is a substantial reduction of detector noise. Preliminary studies made in collaboration with CMS seem to indicate that this effect is due to the coating, eliminating microscopic defects of the plate surface. The possibility to use plates with improved surface is under study.

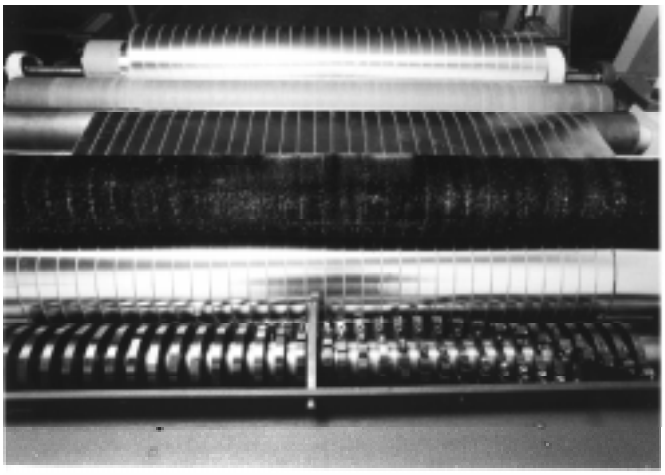

Figure 8-12 The facility used to mill the pick-up strips

The readout strips are made by milling a 40 µm thick aluminium foil glued on a 100 µm thick PET film. A facility with 33 milling heads working in parallel is shown in Figure 8-12. The strips and the aluminium foil for ground reference are glued on the rigid foam core using the hot melt facility already described.

The main mechanical and electrical specifications are summarized in Table 8-3.

Table 8-3 Mechanical and electrical specifications of RPCs

Gas gap	2.00 ± 0.02 mm
Operating voltage	8.90 ± 0.15 kV
Bakelite volume resistivity	$(1–5) \times 10^{10}$ Ω cm
Surface resistivity of the graphite paint	100 ± 40 kΩ
Chamber weight (doublet)	26 kg / m^2
Chamber thickness in radiation lengths (doublet)	8×10^{-2}
Maximum chamber sag due to gravity	15 mm
Leak rate per metre of circumference at 1 mbar overpressure	3 cm^3 / h

8.3 Gas system

8.3.1 Introduction

The main component for the RPC gas is tetrafluoroethane ($C_2H_2F_4$) for the following reasons:

- high density leading to a high primary ionization (~ 60 primary electron–ion pairs per centimetre),
- relatively low operating voltage.

In addition, a small admixture of a hydrocarbon quenching gas is needed.

The RPC chambers comprise a gas volume of 14 m^3 and operate with a gas mixture of $C_2H_2F_4$ / C_4H_{10} (97% / 3%). The basic function of the gas system is to mix the two components in appropriate proportions and to distribute the clean gas mixture into the individual chambers at a pressure of 1 mbar above atmospheric pressure. The hydrostatic pressure gradient of the gas mixture is 0.4 mbar / m, the total height of the RPCs inside the ATLAS experiment is 22 m which makes a compensation of hydrostatic pressure differences necessary.

Table 8-4 Gas system modules

Module	Situated in
Primary gas supplies	SGX building
Mixer	SGX building
Inside closed circulation loop:	
Chamber distribution systems	UXA cavern
Purifier	SGX building
Pump and return gas analysis	USA area
$C_2H_2F_4$ exhaust gas recovery	SGX building

The large detector volume combined with a relatively expensive gas mixture economically justifies a closed-loop circulation system. The system proposed will consist of functional modules, which are designed as far as possible uniformly for all ATLAS gas systems (see Table 8-4). The component sizes and ranges are adapted to meet the specific requirements of the RPC system.

8.3.2 Mixer

The flows of component gases are metered by mass flow controllers, which have an absolute precision of 0.3% in constant conditions (Figure 8-13). Flows are monitored by a process control computer, which continually calculates and adjusts the mixture percentages supplied to the system. This required mixture may either be a constant ratio, or alternatively may be derived from comparison of the running mixture with a reference gas mixture in an analysis instrument. The medium-term stability in constant flow conditions is better than 0.1%; the absolute stability will depend on the absolute precision of the analysing instrument.

Running flows are typically about 30% of full-scale flow. Detector filling would generally be at near full-scale flow, resulting in a volume exchange time of 4 hours.

8.3.3 Closed circulation loop

The RPC chamber gas is circulated in a closed loop with an expected regeneration rate of 90% using in-line O_2 purification. A volume exchange rate of one volume in 12 hours leads to a circulation flow rate of 1.2 m^3 / h and a complete volume renewal every five days.

As shown in Figure 8-14, the circulation loop is distributed over three different areas. Purifier, mixer input, and exhaust gas connections are situated in the mixer room of the SGX building. The compressor and analysis instrumentation are placed in the USA service area. The chamber pressure regulation is done in the UXA cavern near the experiment.

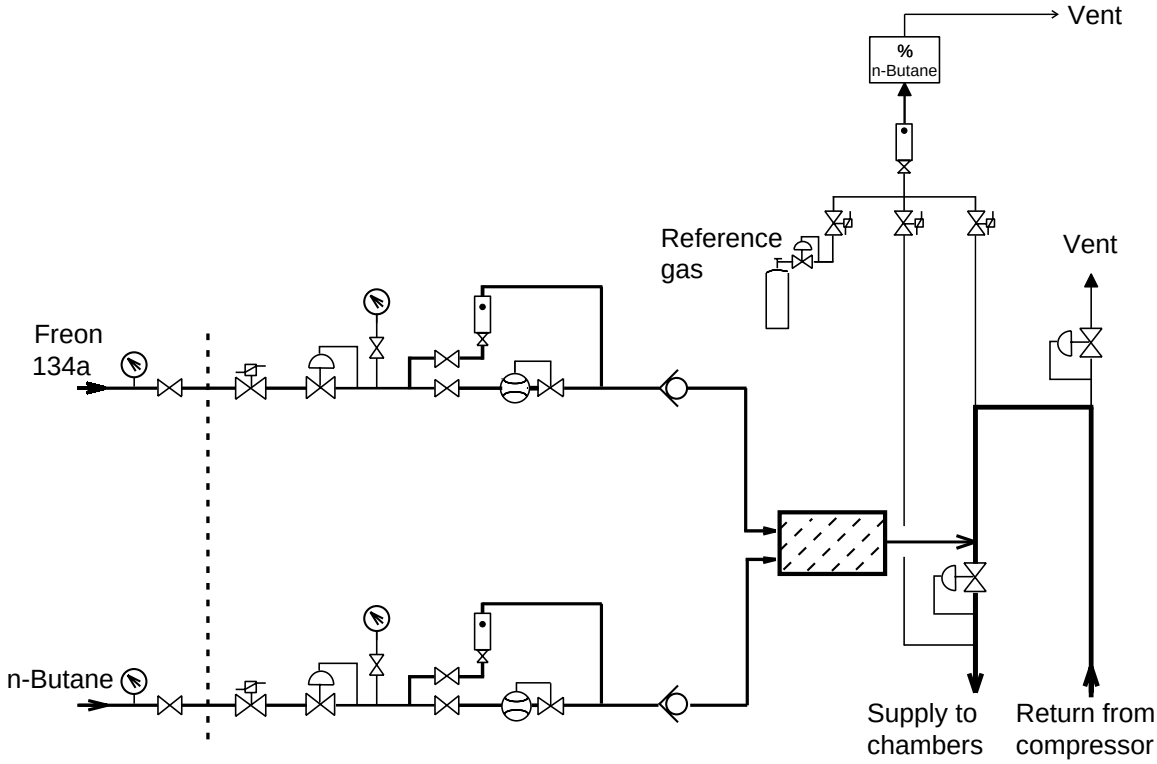

Figure 8-13 $C_2H_2F_4$–C_4H_{10} mixer unit

8.3.4 Chamber distribution system

The RPC detector consist of 596 chamber modules, which are supplied with gas in groups of six, resulting in 96 independent channels. The grouping is arranged such that chambers in different layers of the same sector are not on the same gas channel in order to provide acceptable trigger capacity in case of failure of a single gas channel. Several distribution systems situated in five distinct height zones regulate the chamber pressure relative to the atmospheric pressure, correcting hydrostatic differences. In total, ten racks house the distribution systems, mounted on the wall in the UXA cavern (wall opposite side from USA) at five height levels near z = ±1 m serving the A and C side of the barrel, respectively. They are listed in Table 8-5. This arrangement is the same as in the barrel MDT distribution.

Each distribution system (see Figure 8-15) contains a pressure regulator at the inlet, and a distribution manifold supplying gas to a set of chambers. A needle valve in each line allows the adjustment of individual flow rates. In the output line a back-pressure regulator controls the pressure to +0.5 mbar above atmosphere. The pressure drop in the chamber return pipe is < 1 mbar, leading to a chamber operational pressure of about 1.5 mbar above atmosphere at nominal flow rate.

At the distribution manifolds, every channel has a short flexible pipe with a self-sealing quick connector. This permits gas channels to be individually disconnected from the circulation loop for flushing with inert gas. This facility is also very useful for leak tests on single gas channels.

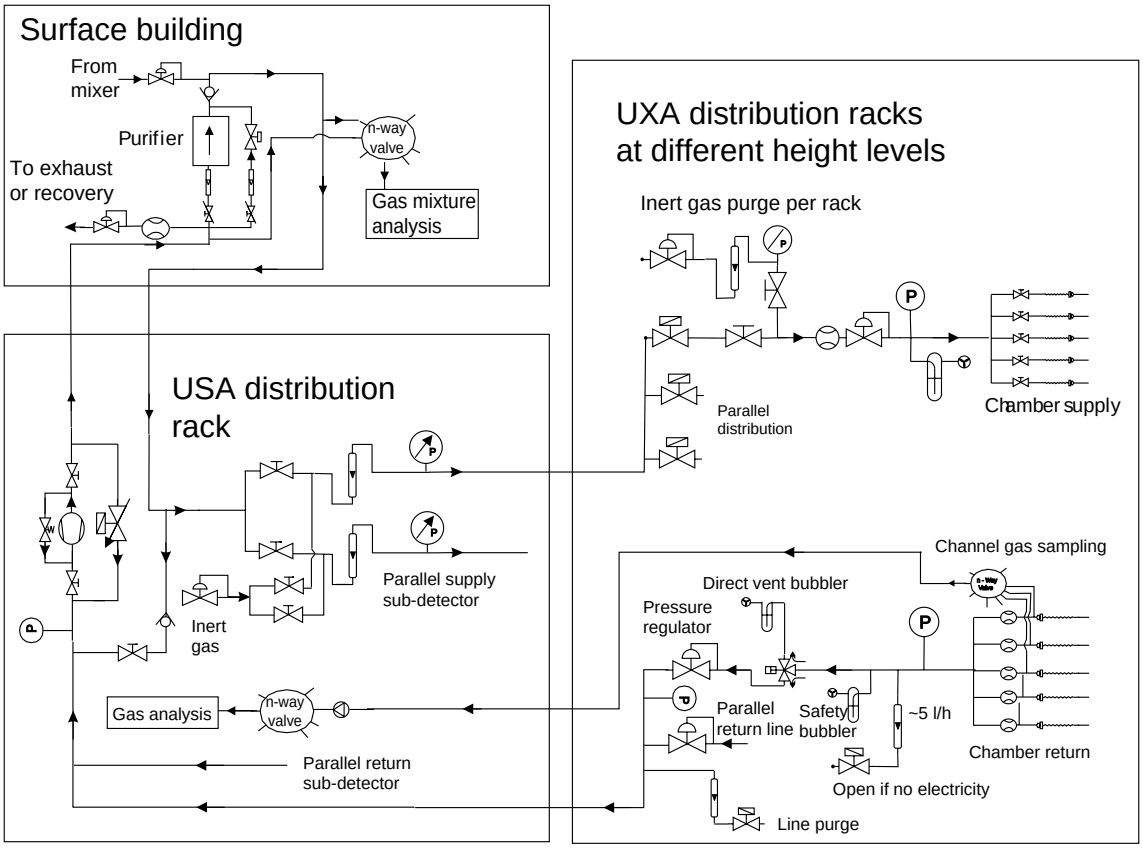

Figure 8-14 RPC gas system overview

Table 8-5 Gas racks for the A side; on the C side, z must be replaced by –z. The third column gives the number of pipe pairs (supply and return), flowmeters and manual regulation valves.

Gas rack name	Location			Channels	Chambers
	x (m)	y (m)	z (m)		
RG.B1.A	13	–10	1	11	BOL..A11, BOS..A12, BMS..A12, BOL..A13, BML..A13, BOS..A14, BMS..A14, BOL..A15
RG.B2.A	13	–5	1	10	BOS..A10, BMS..A10, BML..A11, BML..A15, BMS..A16, BOS..A16
RG.B3.A	13	0	1	6	BOL..A01, BML..A01, BOL..A09, BML..A09
RG.B4.A	13	5	1	10	BOS..A02, BMS..A02, BML..A03, BML..A07, BMS..A08, BOS..A08
RG.B5.A	13	10	1	11	BOL..A03, BOS..A04, BMS..A04, BOL..A05, BML..A05, BOS..A06, BMS..A06, BOL..A07

Every return gas line has a remotely read flowmeter, allowing an easy adjustment of individual channel flows using the needle valve at the inlet. The flow measurement can be used for possible leak detection by observing flow changes in time and by comparing flow rate changes of neighbouring channels. In view of the large number of gas channels, and the fact that the instruments are in a zone which is difficult to access, the flow metering technology must be

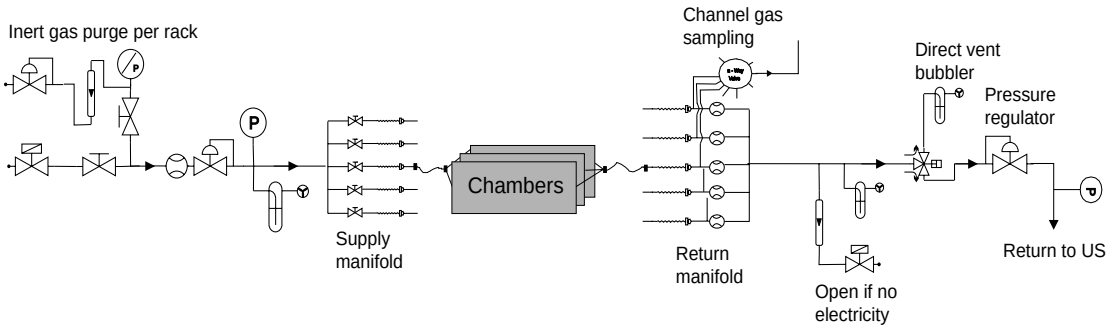

Figure 8-15 Distribution system with chamber pressure regulation

simple, reliable and inexpensive. Currently two measurement principles are being considered: hot-wire anemometers and ultrasonic time-of-flight meters. A choice will be made on the basis of test results and a cost evaluation.

A sensitive indication of gas leaks in a chamber system is an O_2 measurement in the return gas. It is foreseen to sample the chamber output gas in the distribution systems, either channel by channel or for groups of chambers. The sampled gas is sucked back to the USA area with a small pump. Thus gas analysis instruments are accessible at any time and can be shared easily with other detector groups if necessary.

8.3.5 Pump and return pipe pressure regulation

The gas from the distribution systems must be compressed to approximately 100 mbar for return to the surface and recycling through the purifiers. At the same time, the chamber outlet pipe between UXA and USA needs slight underpressure (–5 to –15 mbar) in order to insure correct gas flow through the chambers situated in the bottom part of ATLAS. This pressure can be controlled by a regulation valve in parallel with the pump driven with the signal of a pressure transmitter in the main return pipe.

8.3.6 Purifier

Most closed-loop circulation systems need gas purification in the return line in order to achieve high cycling rates (usually 90%). The principle impurities which may harm the detectors are oxygen, water vapour, halogens and silicones.

For the RPC system, the gas purity requirements are not very high. The oxygen and water levels should remain below 1%, there are no strict limits for the water concentration.

Two standard purifier cartridges, each filled with e.g. a 3 Å molecular sieve and activated copper, can be used allowing water and oxygen removal. The compatibility of the $C_2H_2F_4$ with these cleaning agents remains to be tested; this will be done as soon as the proposed gas mixture is approved.

The advantage of having two parallel cylinders is to run the gas mixture through one of them while the other one is regenerating. The molecular sieve and the activated copper can be regenerated at the same time by heating up the column to 180°C and flushing with an Ar/H_2 (93%/7%) mixture.

The amount of oxygen to be removed is determined mainly by the leak rate of the chambers. The estimated oxygen levels in the return gas suggest a purifier with automated and in-line regeneration.

8.3.7 Distribution pipework

There will be one supply and one return pipe between the SGX building and USA area. Two supply and return pipes connect the USA area to the two barrel detector systems. Taking into account that the distribution racks are at the wall opposite the USA area, the length of these pipe runs is about 170–180 m. The internal detector piping is foreseen in copper with internal diameters of 8 and 10 mm for supply and return line respectively.

8.3.8 Gas recovery

Based on the gas mixture of $C_2H_2F_4/C_4H_{10}$ (97/3), the expected gas cost for eight months of RPC operation is about 90 kCHF (gas prices of 1996). The major part of this is the cost of the tetrafluoroethane. This justifies a recovery of that component since the capital investment for a recovery plant is assumed to be less than a year's $C_2H_2F_4$ consumption. In case the presently proposed gas mixture is confirmed in the future a feasibility study for the recovery of $C_2H_2F_4$ is envisaged.

Table 8-6 summarizes the main gas specifications.

Table 8-6 Gas specifications for RPCs

Gas volume	14 m^3
Concentration ratio $C_2H_2F_4$:C_4H_{10}	(97.0 ± 0.3): (3.0 ± 0.3)
Tolerable contamination: O_2	< 1%
H_2O	< 1%
Gas pressure over atmospheric	(1.0 ± 0.5) mb
Leak rate of the whole system	< 80 l/h
Maximum flow rate	10 m^3/h
Purified gas flow rate	1.2 m^3/h
Fresh gas replenishing rate	0.15 m^3/h

8.4 Electronics

8.4.1 Front-end electronics

An RPC operating in avalanche mode produces typically a single signal of 5 ns FWHM and 1.5 ns time jitter. To preserve this excellent timing information, the pick-up strips which are used to propagate the signal up to the front-end electronics located at the edge of the chamber

must be good transmission lines which do not attenuate the signal amplitude or spoil the timing. It is important to observe that a signal arriving at the front-end electronics after one or more reflections at the ends of the transmission line does not bring any additional timing information but only increases the occupancy. Signal reflections must therefore be suppressed. For this purpose the RPC strip lines are terminated at both ends on their characteristic impedance. As a consequence, only one-half of the charge delivered by the detector is suitable for the front-end electronics. The RPC signal charge values quoted in this chapter represent the charge that is supplied to the front-end circuit.

The detailed layout of a readout strip plane is given in Figure 8-16. The strips are obtained by milling a 40 µm thick aluminium foil glued on a 100 µm thick PET film. This composite aluminium / PET foil is subsequently glued, on the strip side, over a rigid plastic foam plate 3 mm thick that has a second 40 µm aluminium foil, glued on the other face, as a grounded reference plane. The foam sandwiched between the aluminium electrodes is a rigid 'readout panel' that embodies also the front-end board as specified below. Two such panels with strips orthogonal to each other are pressed on the detector gas volume, one at each side. The strips of width ranging between 30 and 40 mm in the different trigger layers are spaced 2 mm from one another and further very narrow grounded strips 0.5 mm wide fixed at the centre of the 2 mm spacing are used for uncoupling contiguous strip signals. According to the described geometry, the resulting strip-line impedance is about 25 Ω, depending on the strip width.

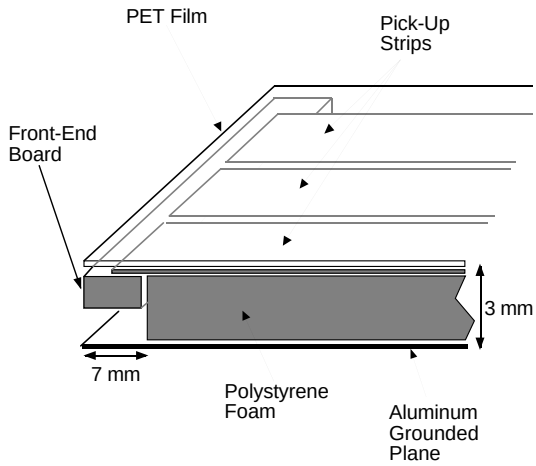

Figure 8-16 Layout of a read-out strip plane

The front-end electronics is based on an 8-channel chip [8-11] which is mounted on boards fixed at the edge of the readout panel between the strip and the ground planes as shown in Figure 8-16. The boards are 3 mm thick to fit the readout panel thickness and 7 mm wide fitting the width of the frame that closes the detector around the edges so as not to decrease the sensitive area of the detector. The length of the boards is tuned with the width of the strips so that each board input is essentially in contact with the corresponding strip and no connection wires are required. The input-to-output delay is the same for all the eight channels.

The front-end circuit is a three-stage voltage amplifier (Figure 8-17) connected to a comparator. It is implemented in a VLSI chip in GaAs technology. The amplifier frequency response was optimized for the typical time structure of the RPC avalanche signal according to the following conditions:

- same risetime for the amplified and the input signals;
- minimum return-to-zero time for the output signal.

The resulting frequency response has a maximum at 100 MHz and a 3 dB bandwidth of 160 MHz as shown in Figure 8-18. The amplifier output is bipolar giving zero integrated charge thus avoiding a possible dependence of the steady output voltage on the counting rate. Figure 8-19 and Figure 8-20 show the simulated amplifier output signals for an avalanche-like

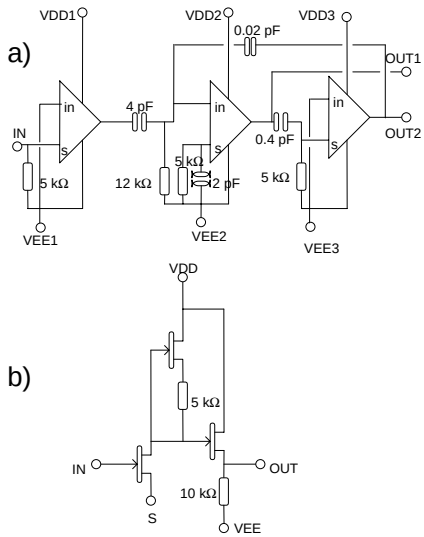

Figure 8-17 Block diagram of the three-stage amplifier: a) interconnection of the three stages; b) sketch of the single stage

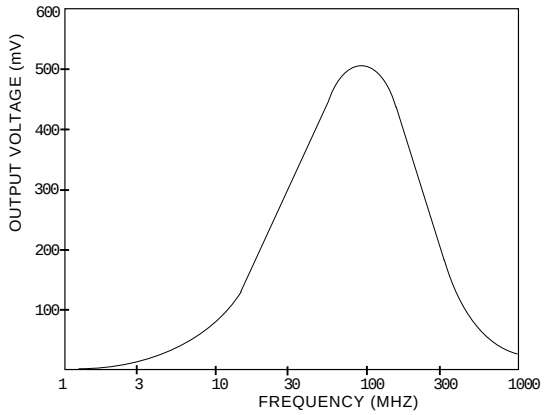

Figure 8-18 Amplifier frequency response simulated with SPICE

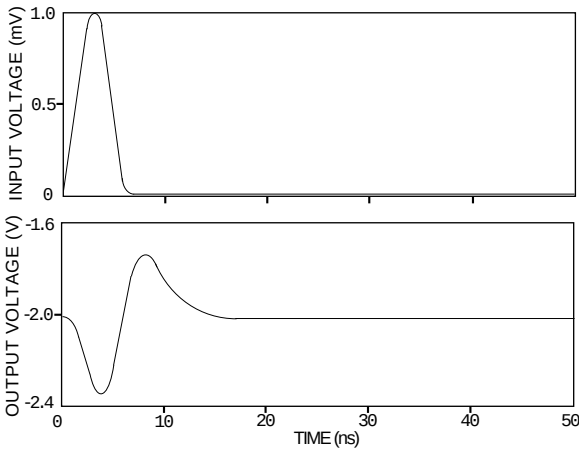

Figure 8-19 SPICE simulated amplifier output (bottom) for an avalanche-like input signal (top)

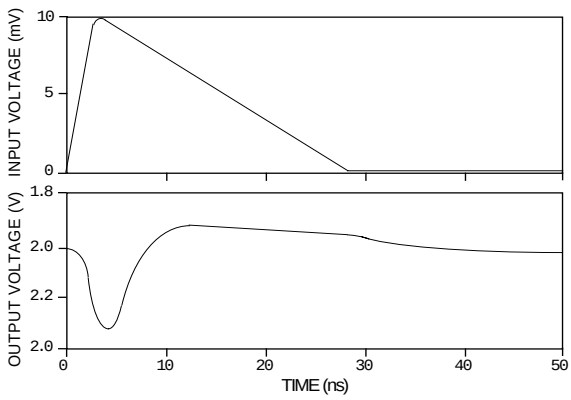

Figure 8-20 As Figure 8-19, for a streamer-like input signal

and a streamer-like input signal. In the latter case the large size of the streamer signal is strongly suppressed and the return-to-zero time is essentially equal to the signal duration. The comparator has a variable threshold which can be set at a minimum value of 50 mV, and a hysteresis cycle of 50 mV giving adequate immunity with respect to the noise. The output is capable of driving a few metres long 100 Ω flat cable connecting the front end to the local trigger logic. The minimum comparator threshold combined with the amplifier gain fixes the minimum detectable signal amplitude at 170 µV.

In Figure 8-21 the simulated comparator output is shown for both a positive and a negative threshold together with the input signal for measuring the input-to-output delay. Owing to the

bipolar amplifier output the same front end can be used for both the X and Y strips that pick up signals of opposite polarity.

A two-channel full-custom prototype chip of the front-end circuit has been manufactured in 0.7 µm GaAs technology. This chip, which is a preliminary step before the 8-channel final version, has been tested on board and also mounted on the detector for cosmic ray tests. The layout of the two-channel chip is shown in Figure 8-22.

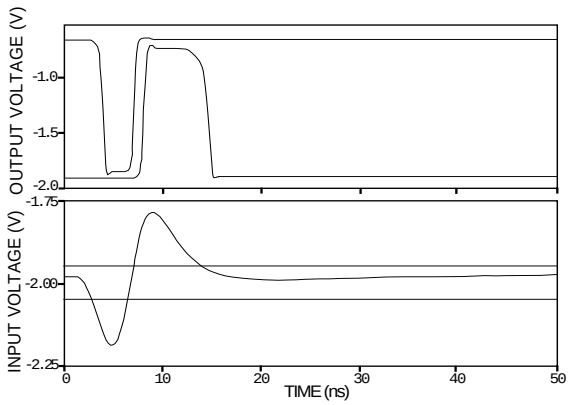

Figure 8-21 Simulated comparator output (top) for a negative and a positive threshold (bottom)

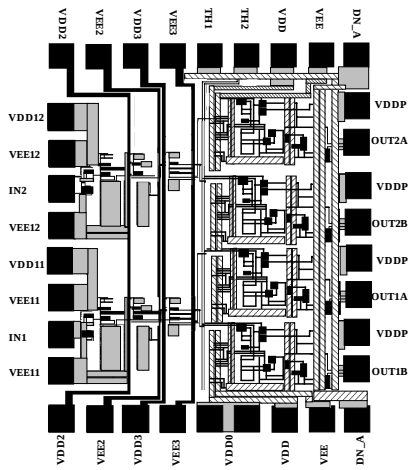

Figure 8-22 Layout of the 2-channel GaAs front-end prototype

Figures 8-23 and 8-24 show the chip output signal observed at a sampling scope giving 0.3 Msample/s with an analog bandwidth of 20 GHz for different amplitude and duration input signals. In both cases a short signal was sent to the B input of the 2-channel prototype and simultaneously a very long (Figure 8-23) or a very high (Figure 8-24) signal was sent to the A input. The A and B outputs are the same in both cases, showing that there is no effect due to the input duration and amplitude on the output signal and there is no cross talk between the two channels.

The expected amplifier noise level for the GaAs front-end can be evaluated according to the following arguments. The r.m.s. voltage thermal noise due to the amplifier input resistance is given by $V_{rms} = (4\ kT \times R \times BW)^{1/2} = 8\ \mu V$. The equivalent noise charge which can be obtained from the voltage noise as $Q_{rms} = t_{peak} \times V_{rms}/R$ is $Q_{rms} = (4\ kT \times t_{peak}/R)^{1/2}$ where t_{peak} is the peaking time. For R values as low as 25 Ω corresponding to the maximum width of the readout strips, we obtain a noise charge of the order of 1 fC. When the strip is connected to the front end, another 25 Ω resistor equivalent to the impedance of the line is put in parallel to the previous one, thus increasing the noise charge by another factor $\sqrt{2}$.

In addition to the thermal noise, another contribution depending on the specific amplifier technology has to be considered. This contribution, which is due to the charge granularity as well as to the parallel input capacitance, is frequency dependent. For a GaAS Mesfet, the minimum value, typically < 1 dB, is obtained at a frequency of about 100 MHz, i.e. in the frequency band of the preamplifier [8-12].

The described tests were carried out on encapsulated prototypes. Further tests are presently in progress for both encapsulated and non-encapsulated prototypes. In the final version of the

front-end electronics non-encapsulated chips will be used. Electronic and signal specifications are summarized in Table 8-7.

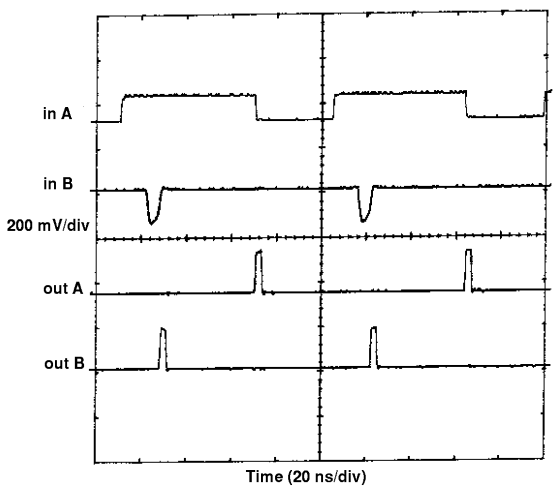

Figure 8-23 Output signals of the 2-channel chip for two simultaneous inputs: a short one in channel B and a long one in channel A

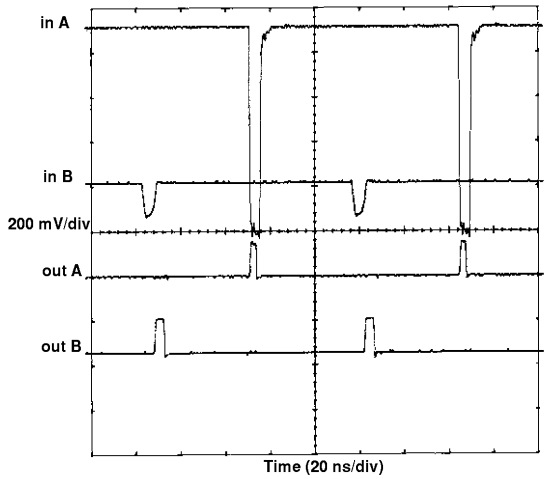

Figure 8-24 Same as in Figure 8-23 with a large amplitude signal in channel A

Table 8-7 Electronic and signal specifications

Total number of channels	368 000
Strip width	30 – 40 mm
Strip line impedance	25 Ω (typically)
Strip length	0.72 – 2.5 m
Signal charge at the amplifier	0.3 pC (peak)
Signal length	5 ns FWHM

8.4.2 The LVL1 muon trigger system

The LVL1 muon trigger [8-13] will be described in detail in the LVL1 Trigger Technical Design Report. In the following we outline the design as it is currently envisaged. It should be noted that the design is not yet final and may evolve between now and the time of submission of the LVL1 Trigger TDR.

The LVL1 trigger system is a pipelined processor running synchronously at 40 MHz and can be subdivided in various parts: some components are on-detector, while others sit in crates either close to the detector or in the underground counting room.

8.4.2.1 The Coincidence Matrix (CM)

The Coincidence Matrix (CM) ASIC, contains both local trigger and readout functions (Figure 8-25). It is mounted on the RPC chamber, very close to the front-end electronics. A group of eight front-end signals, sent on a single cable, is the basic input to the CMs.

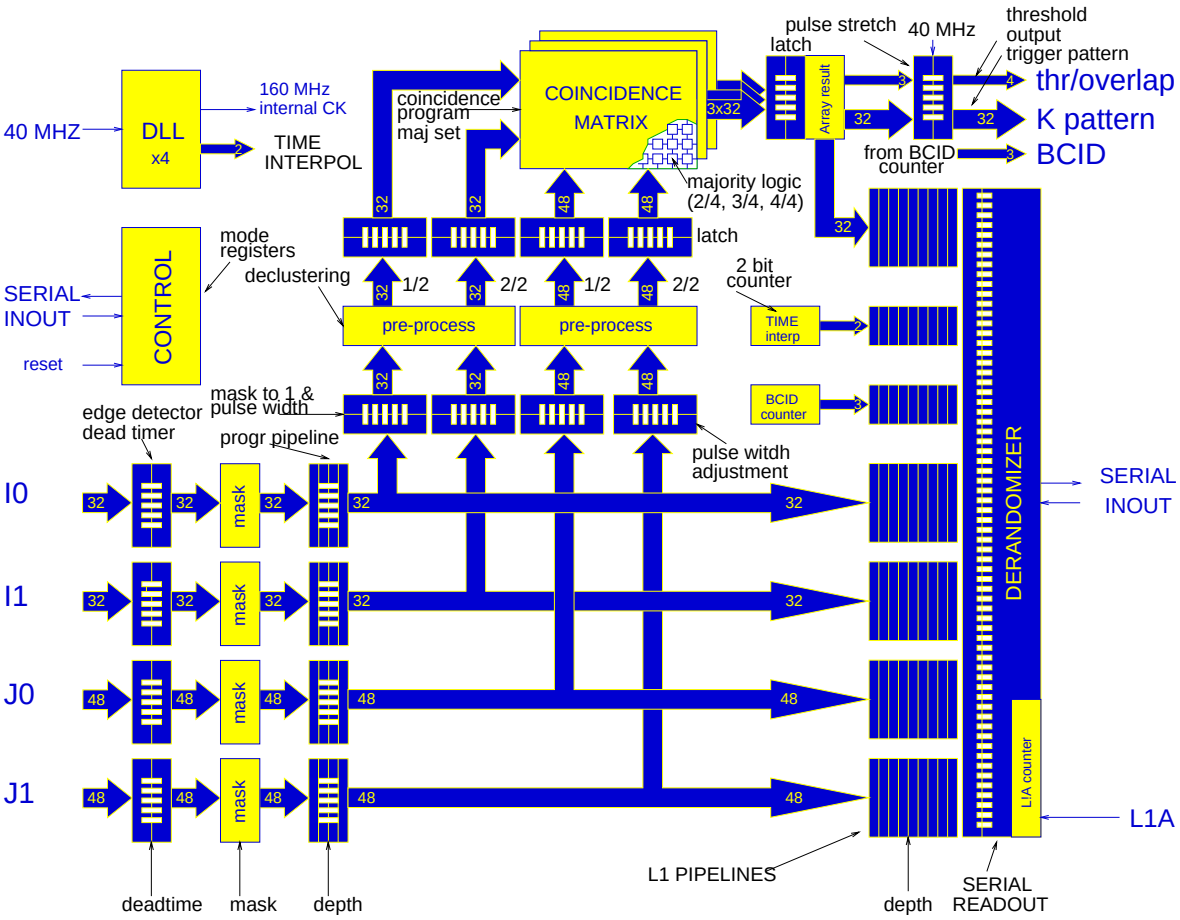

Figure 8-25 Scheme of the ASIC coincidence matrix

The discriminated signals from the RPCs are sampled by the CM every 6.25 ns into pipelines of programmable depth, running at 4×40 MHz. The programmable depth is used to correct for different cable length or time of flight and synchronize the octets of front-end signals with respect to each other. Within each octet, all the propagation times are equalized in the front-end boards. In order to reduce as much as possible the trigger rate due to background hits, the pulses of fixed width coming from the front-end electronics are set at the minimum width, compatible with good coincidence efficiency and considering various effects:

- strip length and position;
- RPC jitter (σ = 1.5 ns);
- interpolator frequency.

Other effects, such as the vertex spread, the trajectory in magnetic field, Coulomb scattering and energy losses have been also considered, but their contribution to the global time spread is negligible.

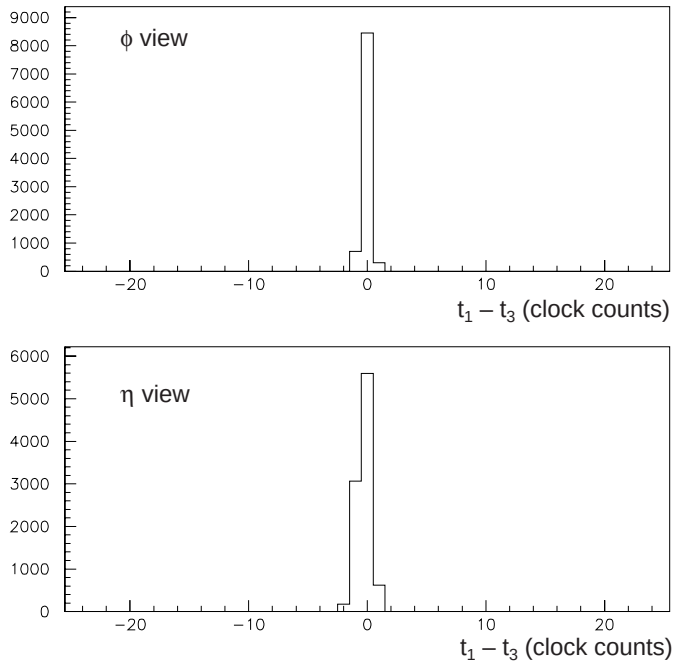

Figure 8-26 Time delay between BML and BOL stations in clock units (6.25 ns) for a 20 GeV p_T muon. The narrower peak in ϕ is due to the shorter ϕ strips.

Figure 8-26 shows the time difference t_M–t_O of the pulses associated with muons of p_T = 20 GeV that cross the middle (M) and the outer (O) stations of the large chambers, in the rapidity region $|\eta| < 1$; both t_M and t_O are evaluated in time bins of 6.25 ns. Similar results have been obtained at different p_T thresholds and for the small chambers.

To ensure full trigger efficiency, allowance for four time bins, i.e. the total width of the η view peak, is needed. The pulse width needed is therefore 2+1 time bins (19 ns); the additional time bin is the resolving time of the coincidence. If a 320 MHz interpolator is considered, the pulse width can be reduced to 12 ns (Figure 8-27).

At present the baseline choice of the time interpolator frequency is 160 MHz, that allows safe BCID and background rejection. A faster interpolator may be adopted if, in the near future, the design technology allows us to build a robust CM running at 320 MHz.

The low-p_T and high-p_T algorithms are realized by programming the same basic CM ASIC.

In the case of the Level 1 Trigger, a frame of n samples is sent to a derandomizing memory, which also does the zero suppression. We expect $n \approx 12$, to cover at least three bunch crossings, during calibration runs, to be reduced during normal runs. The LVL1 readout pipeline, due to the low channel occupancy, could be implemented with a time-stamp technique.

This readout arrangement will be capable of assigning an RPC hit a time value with an r.m.s. resolution of $25\ \mathrm{ns}/(4 \times \sqrt{12})$, comparable to the RPC time resolution. Such a scheme is necessary to monitor the performance of the detector during the data taking and to minimize background in analysis.

We will build only one type of CM and associated board. The board uses 160 front-end inputs in the case of the M station and 128 front-end inputs in the case of the O station. Each CM board has an asynchronous readout link. The readout system will be described later.

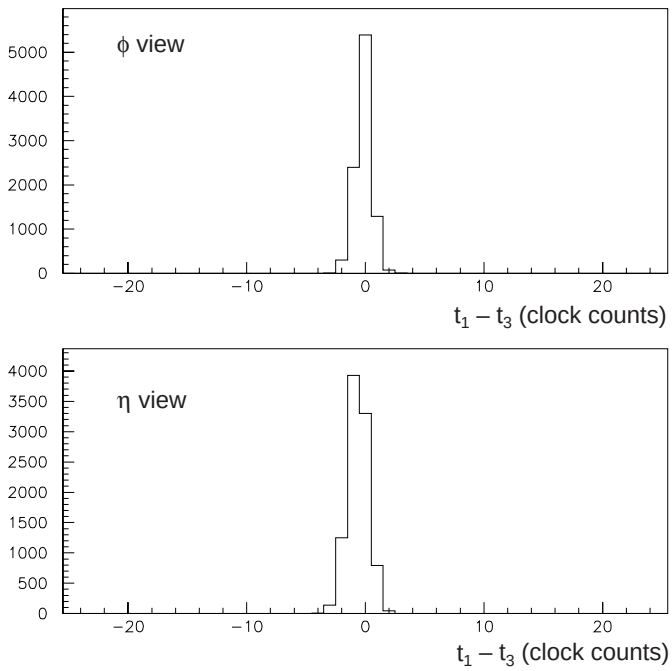

Figure 8-27 As Figure 8-26, with the time scale in units of 3 ns (320 MHz clock)

8.4.2.2 Pad Logic (PL)

Two CMs and related electronics, implementing both low-p_T and high-p_T algorithms on a single projection define the trigger Local Logic (LL).

Each LL unit selects muon candidates in the r–ϕ and r–η planes independently, every 25 ns. The association of the muon candidates to Regions Of Interest is done by the Pad Logic (PL). Each PL module, looking at four LLs, covers four $\Delta\phi \times \Delta\eta \sim 0.1 \times 0.1$ ROIs (Figure 8-28). Each PL can identify without ambiguity the ROI of up to one muon candidate, identify multiple tracks, and solve ambiguities of tracks in overlapping regions of two CMs.

Two types of PL boards are required, low-p_T PLs and high-p_T PLs. The low-p_T PLs have only the readout link, an asynchronous serial link running with a bandwidth requirement of 10 Mbit/s. The high-p_T PL boards contain the readout link and the trigger output, a 16 bit synchronous link running at 40 MHz. The PL boards will be mounted on detector.

The circuits of the trigger LL are located on the RPCs as shown in Figure 8-28.

8.4.2.3 Sector Logic (SL)

Each small (large) sector contains 7 PL boards, made of 22 (24) r–ϕ LLs and 28 (28) r–η LLs. A trigger sector covers half of the whole barrel region in pseudorapidity and a $2\pi/32$ region in ϕ.

In the present design the Sector Logic (SL) modules are located around the detector, at $\eta = 0$, close to the BO chambers. Each SL module receives information from each PL on a separate link, as described above.

Each SL sorts the muon candidates by p_T and selects up to two tracks per sector. We have in total 64 SL boards. Each SL is also able to solve double counting of tracks passing in the overlap regions between two PLs and to flag tracks going in the barrel end-cap boundary regions. The 32 -bit outputs of each SL are sent to the Muon Central Trigger Processor (MCTP) every 25 ns via synchronous links. The trigger data links among Pls, SL and MCTP are shown in Figure 8-29.

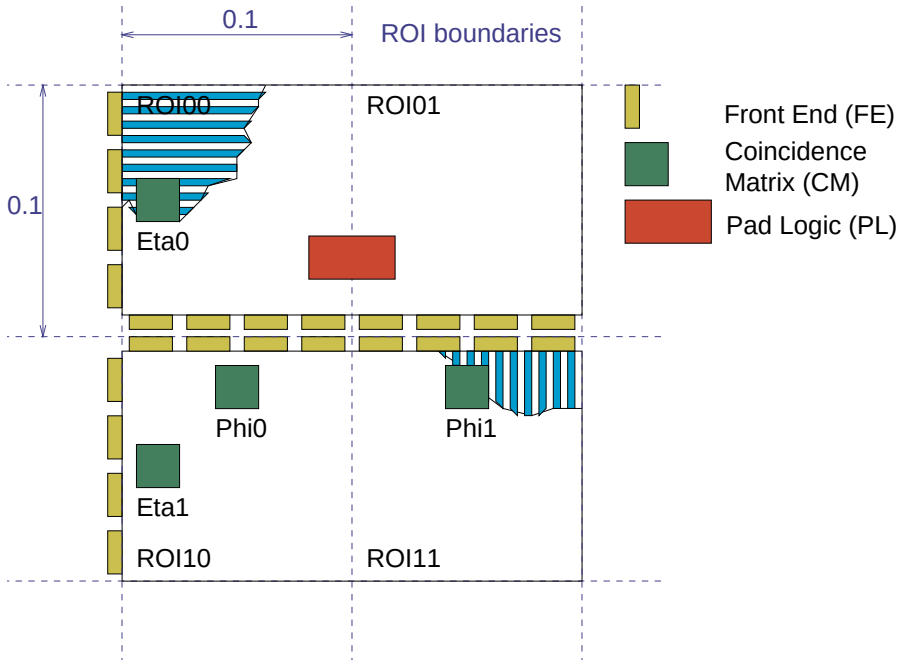

Figure 8-28 Position of the local trigger logic circuits on the RPCs

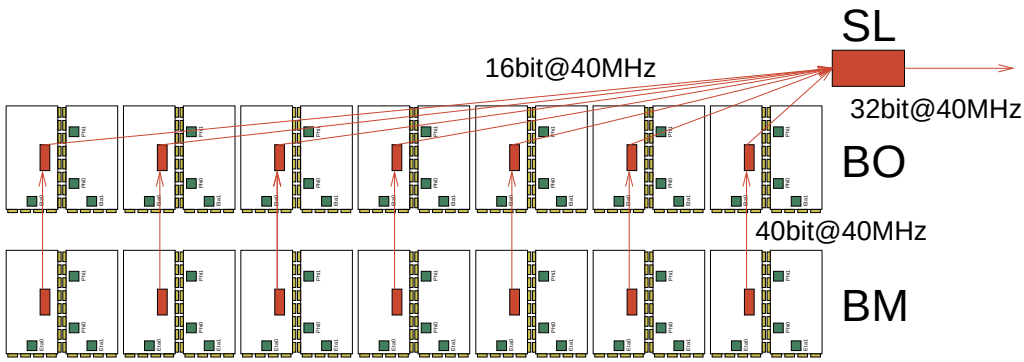

Figure 8-29 Scheme of the trigger data links among Pad Logics, Sector Logic and Central Trigger Processor

8.4.2.4 Muon Central Trigger Processor (MCTP)

The muon trigger processor has two functions:

- it solves ambiguities of muon candidates in boundary regions on the barrel and between the barrel and the end-cap;
- it classifies and counts the muon candidates from the barrel and the end-cap trigger systems, as necessary for the LVL1 Central Processor and ROI builder.

The current design foresees 368 k detector channels, 3264 CMs, 896 PL and 64 SL boards.

8.4.3 The readout system

8.4.3.1 The readout tree

The RPC readout is based on the data concentration from the PL boards. Sixteen Readout Drivers (RODs) are foreseen for these data, eight for the small and eight for the large chambers.

Each PAD board concentrates data from four CM boards, daisy-chained via a low bandwidth serial link. Each ROD concentrates data from the 56 PADs corresponding to the RPCs and trigger logic distributed on a large (small) BM and BO station, in the entire barrel. Each ROD sends both chamber and trigger data to the readout. With this assumption, the data are collected in a readout tree which matches closely the precision chamber readout at the level of the Readout Buffer (ROB).

Alignment of data packets belonging to the same event is done at each level of data concentration. Event ordering is maintained to facilitate event handling and checking. Some synchronization checks are done at the ROD level to ensure data integrity.

Data from each ROD are transferred to a corresponding ROB in the readout crates located in counting rooms and are kept there for the LVL2 latency.

Data from precision chamber ROBs and from trigger chamber ROBs are stored in the same readout crate if they belong to the same tower.

The initialization of the readout and trigger electronics is done via dedicated lines of the Trigger and Time Control System or by Detector Control System (DCS) lines.

All these trigger and readout components have to be initialized and monitored.

8.4.3.2 Data format and bandwidth requirements

The data format will follow closely the lower level hardware organization, based on coincidence matrices. Channels belonging to overlapping trigger windows will be handled as independent information; data will be repeated.

The proposed data format includes zero suppression at the LL, PL and SL levels. Data belonging to a single SL will be sorted in the following way: low-p_T LLs followed by high-p_T LLs. The four r–η followed by the four r–ϕ matrices, with LL data organized as shown in the trigger chapter.

The amount of RPCs and trigger data going to central readout can be conservatively estimated as follows. With the proposed data format, 24 bytes will be necessary to identify a muon candidate, including summary information, headers, and IDs. Given a 10 kHz inclusive muon rate,

the required trigger data bandwidth will be about 2 Mb/s, to be added to the raw RPC strips data.

The RPC data volume can be estimated assuming a signal shaping time of 20 ns, a background rate of 100 Hz/cm^2, an average strip length of 200 cm and a pitch of 4 cm, giving an estimated channel occupancy of about 2×10^{-3}. Assuming 368 k strips and a ~100 kHz average trigger rate, we get 4×10^7 hits/s for the small and 5×10^7 hits/s for the large sectors.

Assuming that we make zero suppression, encoding each hit in 2 bytes, we get a total of ~ 2 kB/event, to be compared to ~ 60 kB/event if no zero suppression is applied. The additional bandwidth for data from the trigger logic is negligible after the zero suppression

8.4.4 Power consumption

The power consumption per channel for the on-detector electronics is estimated as follows:

- 30 mW front-end;
- 40 mW trigger and readout.

These numbers are calculated on the assumption that all the copper interconnections are done with LVDS levels, to reduce power. The total on-detector power consumption is 28 kW. The sector logic uses 16 crates with an estimated power consumption of 1.5–2.2 kW per crate.

Water cooling can be used for on-detector and off-detector electronics if needed. Different systems are under study.

8.5 Test of prototype performance

8.5.1 Beam and cosmic ray tests

An exhaustive programme of chamber prototype testing [8-6,8-14,8-15] has been carried out in the RD5 experiment [8-16] at CERN and with the ATLAS H8 test-beam facility in the SPS North Area at CERN. The programme was driven mainly by two needs:

- to study the basic characteristics of the detector working in avalanche mode;
- to test the performance of the first-level muon trigger logic and processor.

Most of the chambers to be tested were therefore arranged according to the ATLAS trigger scheme which is based on trigger ‘towers’ made up of three stations: two middle stations for the low-p_T trigger and the outer one for the high-p_T trigger (Figure 8-30).

A small-sized (50×50 cm^2) and a full-sized (270×90 cm^2) trigger tower prototype were built and tested on the H8 beam [8-17]. Muon and pion beams up to a maximum flux of 500 Hz/cm^2, distributed over a 10×10 cm^2 area, were used in this test. The beam trigger signal was provided by scintillator counters of various dimensions (2×2, 4×4, 10×10 cm^2).

A precise reconstruction of the muon tracks along the horizontal direction was obtained by means of two trackers made up of 3 cm diameter drift tubes. Each tracker consisted of 16 tubes

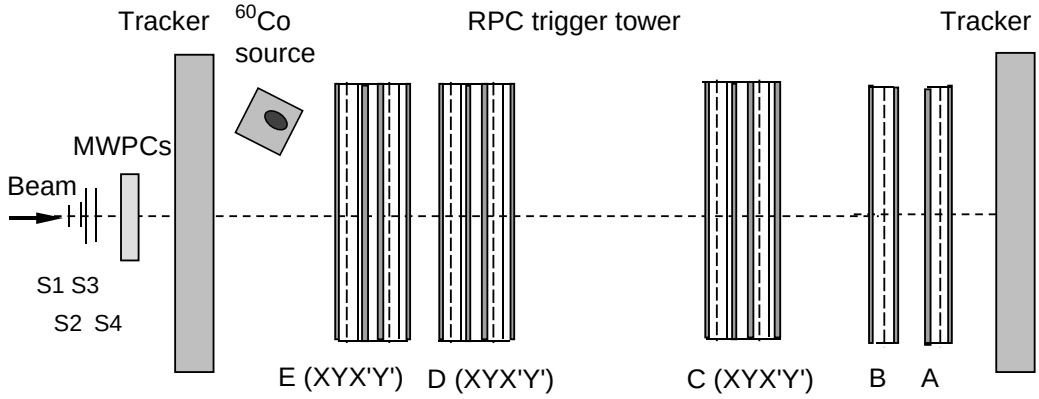

Figure 8-30 RPC chamber layout in the H8 test-beam facility

disposed on four layers and oriented along the vertical direction. Both towers consisted of six single-gap RPC chambers, arranged in three stations of two chambers each. These 'doublets' were located along the beam line, two at a distance of 40 cm from each other and the third 200 cm downstream with respect to the second one in order to simulate the ATLAS low-p_T and high-p_T first-level muon trigger schemes. With the purpose of simulating the low-energy LHC background conditions, a 14 mCi ^{60}Co source was used to irradiate the upstream RPC layer with a photon flux giving a 100 Hz / cm^2 counting rate spread over most of the detector area.

The RPC chambers were read out on both sides by 31 mm pitch strips, orthogonal to each other, according to the ATLAS trigger scheme. The front-end electronics consisted of a two-stage voltage amplifier with a gain of about 300 and a bipolar output signal. The amplified strip signals were sent to discriminators with threshold adjustable between 15 and 300 mV. This threshold was set at 100 mV for the Y strips and 200 mV for the X strips. The different thresholds were needed to compensate for the different gains of the inverting (X strips) and non-inverting (Y strips) front-end amplifiers. The discriminator outputs were sent either to input registers for pattern reconstruction or to 1 ns resolution TDCs for time measurements.The detectors were operated in avalanche mode. In addition to the trigger towers, two 50×50 cm^2 RPCs with similar characteristics (2 mm gas gap), were installed on the beam to study specifically the charge distribution as a function of the operating voltage and the transition from the avalanche to the streamer regime. The strips from these chambers were read out at both ends to study the avalanche and streamer charge distributions at the same time. The signal from one end of the strip was directly sent to the input of an ADC module to measure the streamer charge which is big enough not to require amplification. The long duration of the gate signal (250 ns) allowed for possible long delays of the streamer. The signal from the opposite end of the same strip, was first amplified and then sent to a second ADC for avalanche-charge measurement. The gate signal in this case was only 70 ns long to exclude possible streamer signals usually occurring at a much later time.

The measurement of the detector performance in the tests of the two prototype towers concerned the following parameters:

- efficiency;
- time resolution;
- cluster size;

- tracking accuracy;
- response uniformity over the full chamber area;
- avalanche charge;
- streamer probability.

The combined performance of the detector and the trigger processor is presented in Section 8.5.2.

The chambers were operated with a gas mixture of isobutane and tetrafluoroethane.

In Figure 8-31 the RPC detection efficiency and streamer probability are reported as a function of the operating voltage for a 50×50 cm^2 doublet at a beam flux of 500 Hz/cm^2. The data refer to two different gas mixtures, iso-C_4H_{10}/$C_2H_2F_4$ in ratios of 6%/94% and 1.6%/98.4%.

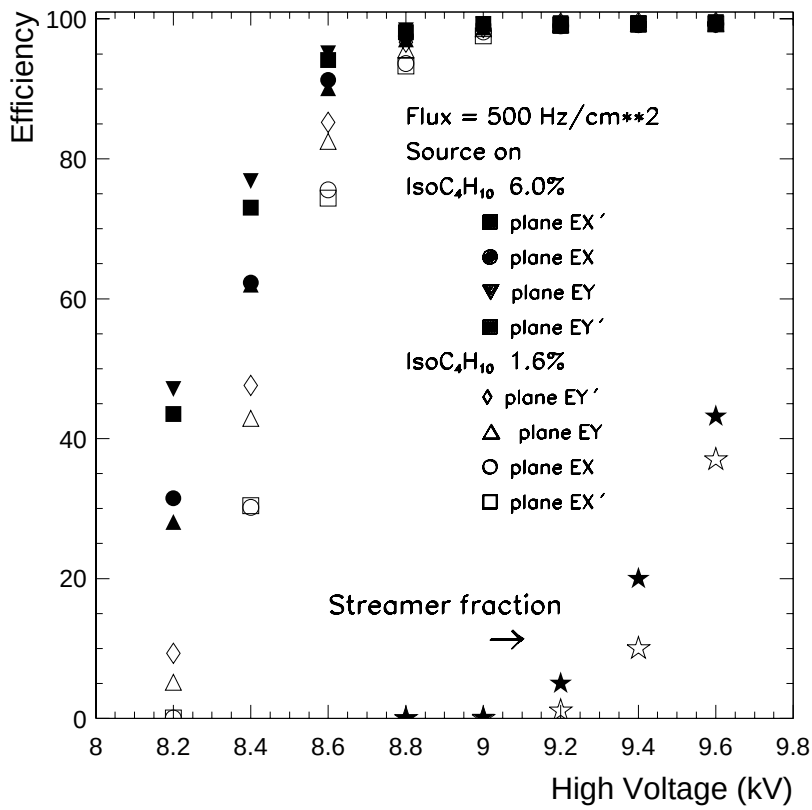

Figure 8-31 Detection efficiency and streamer fraction vs. operating voltage for a 50×50 cm^2 doublet. Each doublet consists of four strip planes (X, Y, X′, Y′). The closed and open symbols refer to 6% iso-C_4H_{10} and to 1.6% iso-C_4H_{10}, respectively.

The efficiency vs. operating voltage for a full-sized chamber, at a muon beam flux of 350 Hz/cm^2, is shown in Figure 8-32.

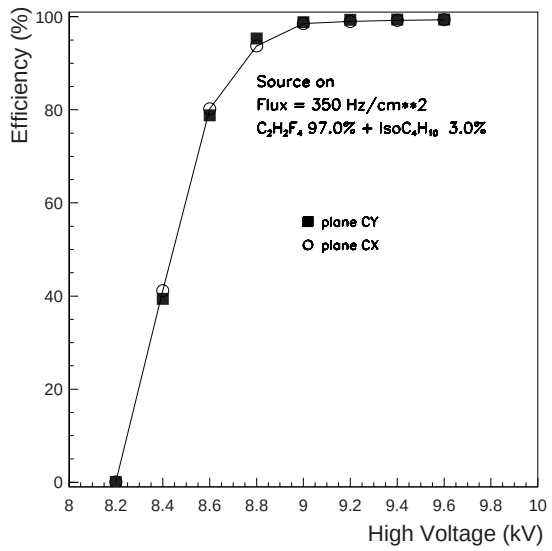

Figure 8-32 Detection efficiency vs. operating voltage for a full-sized chamber

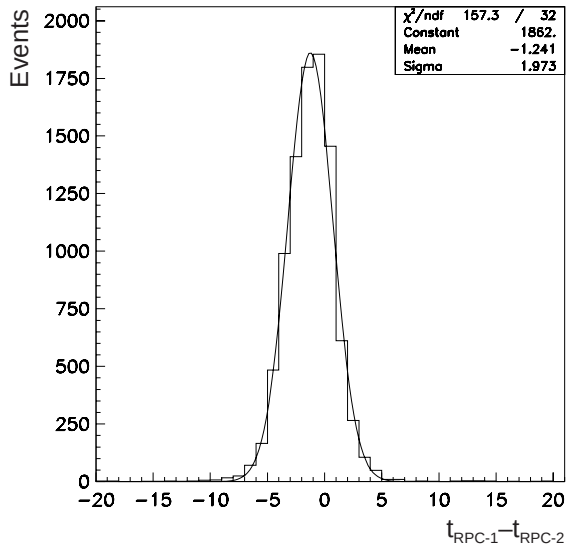

Figure 8-33 Distribution of the time of flight between two RPC chambers

In the latter case the amount of isobutane in the gas mixture, 3%, was well below the flammabil-

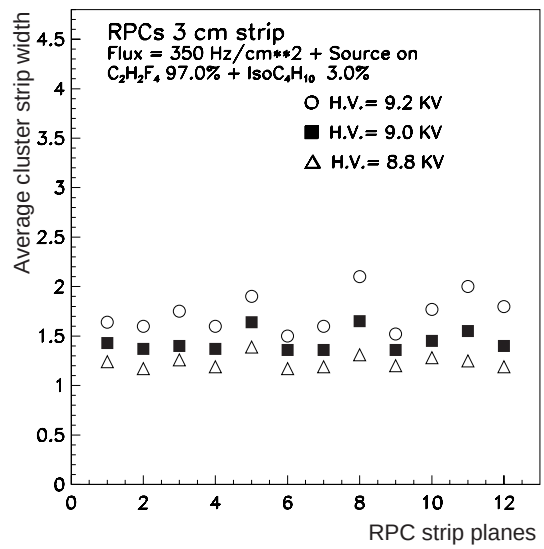

Figure 8-34 Average cluster size for the 12 strip planes of the big RPC trigger tower.

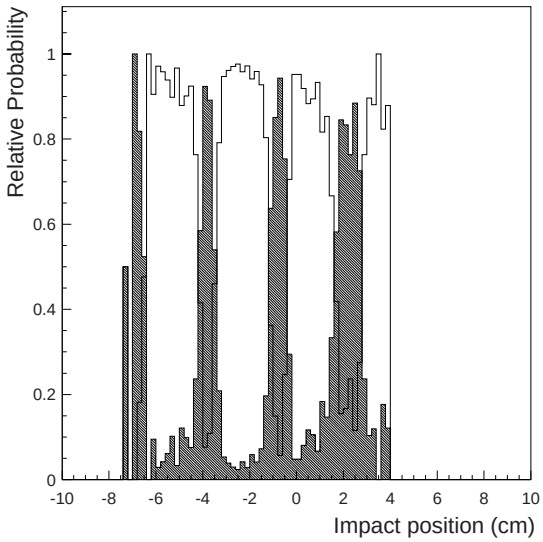

Figure 8-35 RPC hit probability vs. reconstructed hit position for events of cluster size 1 (open histogram) and 2 (shaded histogram).

ity threshold which is about 5.7% [8-18]. The same mixture was used for all the results presented below.

The distribution of the time of flight between two RPCs of the tower is shown in Figure 8-33. From a Gaussian fit of this distribution we extract a σ = 2 ns, corresponding to a single-layer time resolution of about 1.5 ns, well below the 25 ns LHC bunch-crossing period.

Figure 8-34 shows the average cluster sizes for the six RPC planes of the full-sized trigger tower (twelve strip planes) at voltages of 8.8, 9.0 and 9.2 kV. The average cluster size, namely the number of contiguous hit strips per event, is 1.5 at 9.0 kV. With the purpose of correlating the observed cluster size with the track position, we have reconstructed the muon trajectories by means of the external trackers. The position distribution of the track impact point is presented in Figure 8-35, for events with cluster size 1 and 2 respectively. The distribution pattern fits the 3 cm strip pitch: events with cluster size 2 are occurring when the particle hits the detector in a region of about ±5 mm around the edge of two contiguous strips, while the cluster size is 1 when the strip is hit within ±1 cm from its centre.

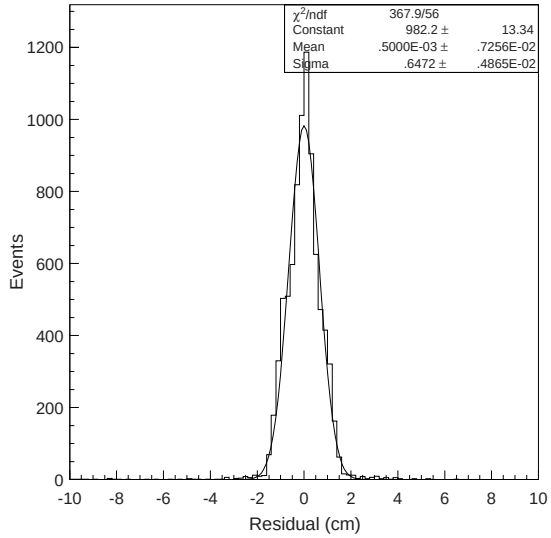

Figure 8-36 Distribution of the RPC residuals with respect to the reconstructed hit position.

Figure 8-36 shows the distribution of the residuals coming from a straight line fit of all tracks crossing the full-sized trigger tower (six RPC chambers in both views). The spatial resolution obtained is about 6 mm.

In each of the tests described so far the maximum detector area that could be tested in a single run was limited by the actual size of the muon beam which was about 100 cm^2.

In order to extend the test of the full-sized chambers over the largest possible area, the beam halo was used. The halo trigger was given by the coincidence of two large-area scintillator hodoscopes each made up of five scintillators of size 10×100 cm^2. In the halo test the muon tracks were reconstructed using four out of the six RPC layers according to the following procedure. Each RPC was tested using, among the halo triggers, only the events showing a hit in all the four layers belonging to the doublets not containing the layer under test. The detected hits were required to fit a straight line in both the x and y views with the condition of a χ^2 probability bigger than 0.01. For each event fulfilling the above conditions, the reconstructed muon track was intersected with the layer under test. This was considered efficient if a cluster aligned with the muon trajectory was detected.

Figure 8-37 shows the x–y distribution of all the impact points extrapolated from the muon tracks. A high density region is visible around the centre of the figure due to the ordinary beam. The hodoscope trigger logic, indeed, did not require the beam veto.

The level curves of the x–y distribution of the impact points for events in which no hit was found in the RPC layer under test is shown in Figure 8-38. These points are concentrated around regularly spaced positions fitting the spacer pattern very well.

The avalanche charge distributions obtained in a cosmic ray test are shown in Figure 8-39 for operating voltages ranging from 8.5 kV to 9.0 kV in steps of 100 V. At 8.5 kV the distribution shows an exponential-like behaviour as expected for proportional mode operation. At 9.0 kV a peak is clearly visible, suggesting saturated avalanche mode operation.

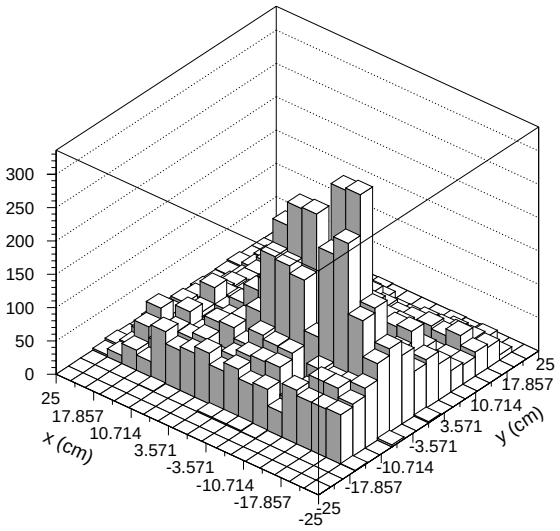

Figure 8-37 x–y distribution for all reconstructed hits

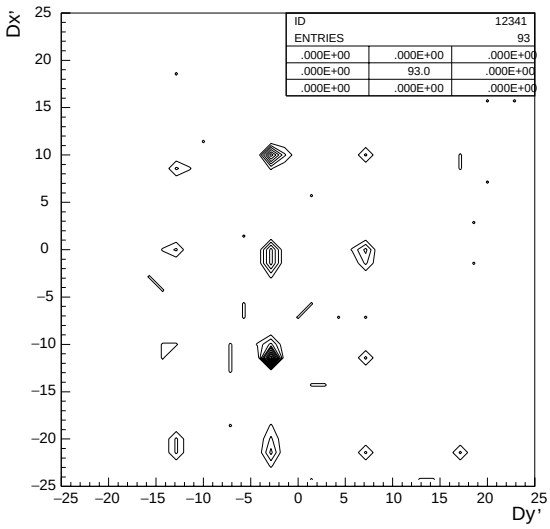

Figure 8-38 The x–y distribution of the reconstructed hits corresponding to RPC inefficiencies

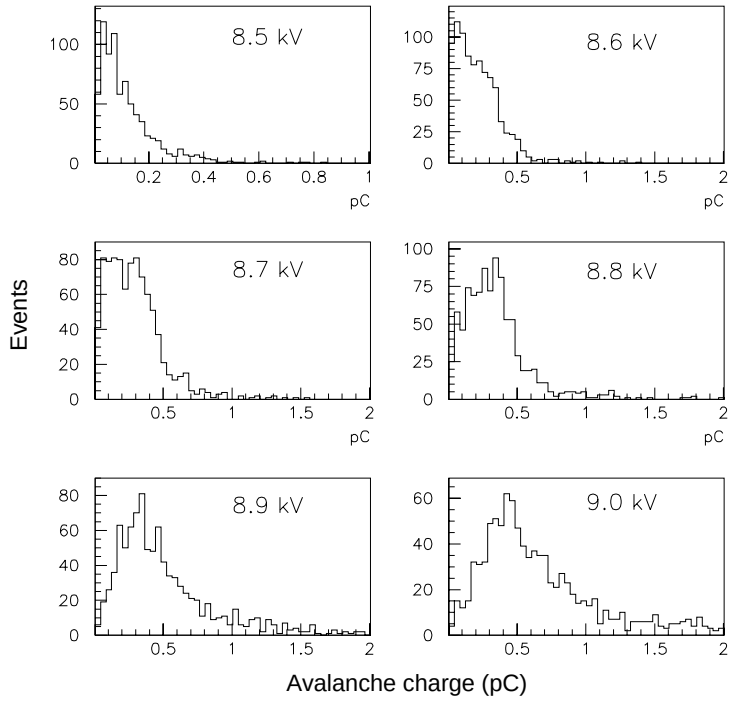

Figure 8-39 Avalanche charge distributions at different operating voltages

Long-term cosmic-ray tests have shown fluctuations of the efficiency plateau knee of the order of ± 100 V, which turned out to be correlated with changes of the atmospheric pressure and laboratory temperature. These fluctuations disappear if the operating voltage is corrected so as to keep the field-to-gas-density ratio constant. An online correction of the high voltage to compensate for temperature and pressure fluctuations is foreseen.

8.5.2 Trigger demonstrator

Two trigger demonstrators have been built and tested in various configurations [8-19]. A coincidence matrix ASIC, with all the trigger functionalities, has been developed and mounted on a VME board and tested. During the 1996 test beam period, on the H8 beam line, six chambers were arranged in three doublets and equipped with eight CMs, to simulate a 2×2 ROI PAD.

Each chamber was equipped with 16 front-end channels. The low-p_T trigger processing was done on each view by programming two CMs, using signals from the first doublet as input. The high-p_T trigger processing used the output of the low-p_T CMs and the front-end signals from the third doublet; it was done by two CMs per view. The measured processing time and jitter of the electronics is shown in Figure 8-40.

The trigger efficiency is shown in Figure 8-41, together with the efficiency of the single chambers.

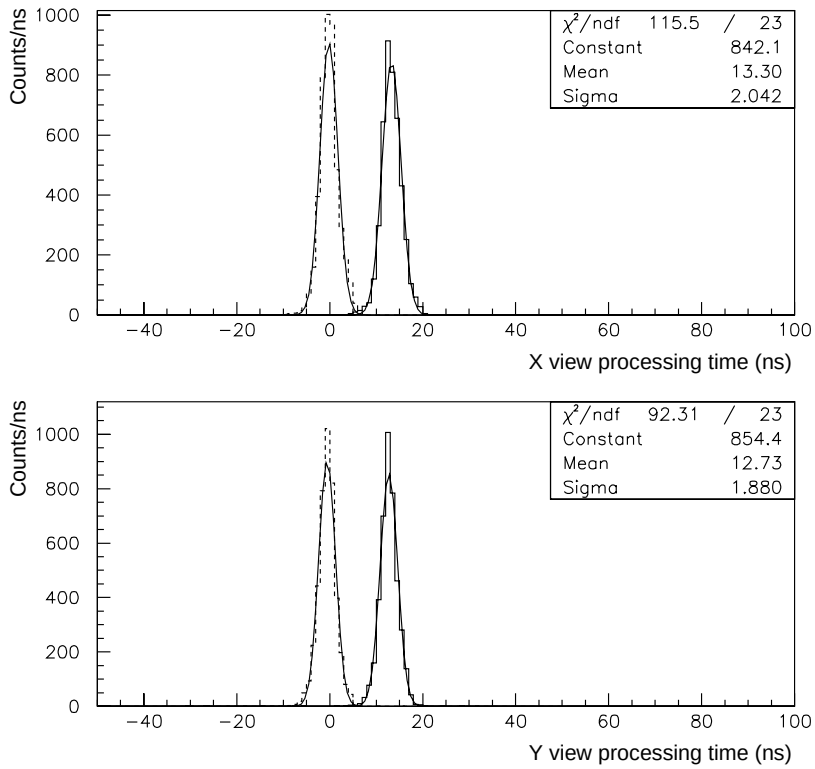

Figure 8-40 Processing time jitter of the LVL1 trigger processor for low-p_T (dashed histogram) and high-p_T (full histogram) tracks, for both the X and the Y coordinate. The average low-p_T processing time is subtracted such that the distribution is centred at t = 0.

8.5.3 Ageing test

With the purpose of searching for possible ageing effects induced on the RPCs during 10 years operation at the LHC, an ageing test was performed on a 10×10 cm^2, 2 mm gap RPC which was irradiated with 1.3 MeV photons from a 4 mCi ^{60}Co source.

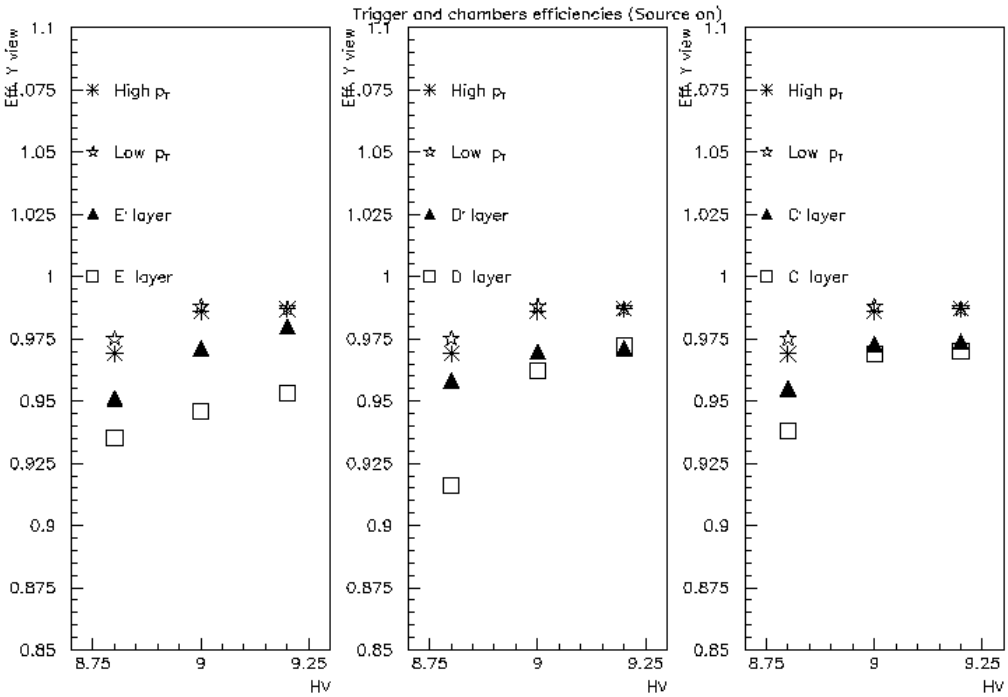

Figure 8-41 Comparison of the LVL1 trigger efficiencies to the single chamber efficiencies for the full-sized test trigger tower

The experimental set-up consisted of a lead box containing the source and the chamber under test. The source was fixed at the end of a long screw, crossing the box upper wall, which allowed the distance between the chamber and the source to be changed during the test. The chamber was irradiated with the source 3 cm above it.

During the irradiation the chamber was operated in avalanche mode using a gas mixture of 97% tetrafluoroethane and 3% butane. The operating voltage was set at 9.0 kV and the discrimination threshold was 30 mV during the full test period.

The efficiency was measured using cosmic muons selected by a tracking trigger system consisting of two x–y RPC stations located above and one station located below the lead box.

The tracking capability of the test chamber is shown in Figure 8-42, where the distribution of the residual of the hit with respect to the trigger track is plotted. The chamber was irradiated for 2.5 months at a typical rate of about 200 kHz corresponding to an average of 2 kHz / cm^2. The total number of counts per unit area, integrated during the test period and averaged over the chamber sensitive area, corresponds to 10 years of LHC operation (10^7 seconds / year) at a measured flux of 100 Hz / cm^2.

The chamber counting rate, which was continuously monitored during the test, is shown in Figure 8-43. Two effects are evident:

- a number of rate fluctuations on the scale of several days which are present over the full test period;
- a decrease of the average rate during the first half of the testing period.

The rate fluctuations are due to changes in atmospheric pressure and temperature which affect the ratio of the electric field to the gas density. Indeed at the test rate, which is about 100 times larger than the value expected in the ATLAS barrel, the operating voltage of 9.0 kV is below the efficiency plateau.

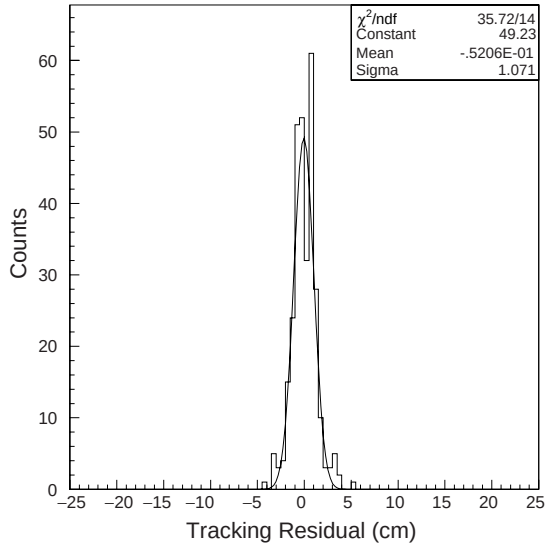

Figure 8-42 Distribution of the hit residual with respect to the triggered track

The average rate decrease at the beginning of the test indicates a reduced rate capability of the chamber. However this is a relevant effect only at much higher rates than the ones expected in the ATLAS barrel. With the purpose of checking the chamber performance in realistic conditions, after the ageing test we increased the distance of the source up to the point in which the counting rate was 100 Hz/cm^2, i.e. the rate expected in ATLAS multiplied by a safety factor of 5. The detection efficiency, at the same operating voltage and discrimination threshold used in the test, was found to be $(98 \pm 1.5)\%$ to be compared with the value of $(97 \pm 3)\%$ which had been measured at the beginning of the test.

In the efficiency measurement we selected tracks with acceptable scattering angles measured with the external tracker. This condition was required to reduce the probability of accepting triggered tracks which did not cross the test chamber inside the sensitive area. The resulting statistics of the accepted events is therefore modest and this explains the large statistical error.

We conclude that at the level of the ATLAS performance required for the RPCs no ageing effect was detected in the test.

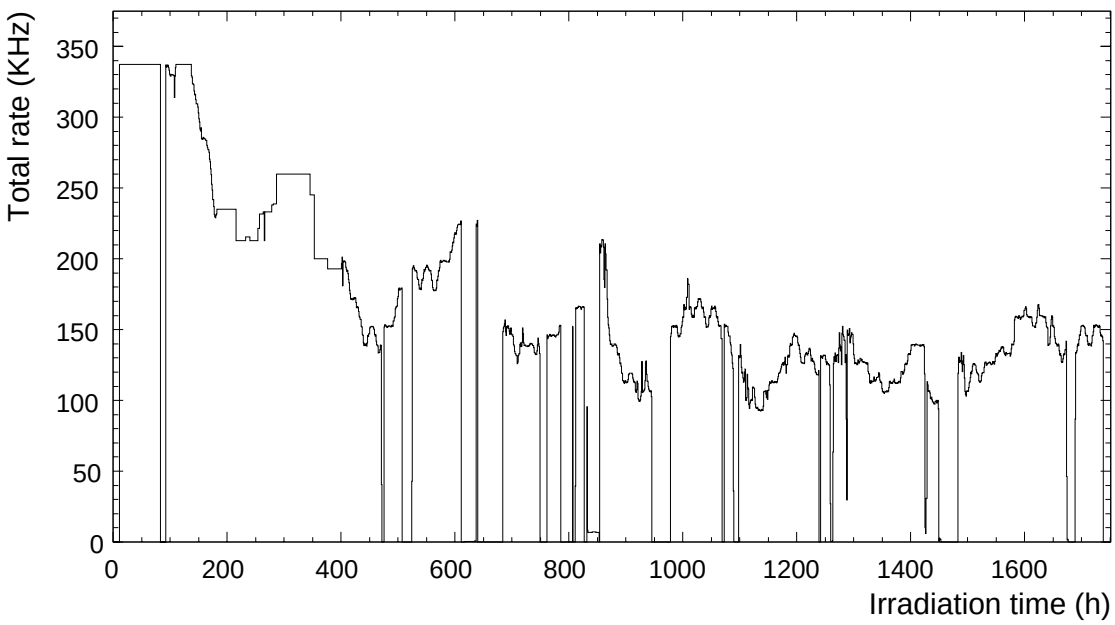

Figure 8-43 Test chamber counting rate as a function of the irradiation time

8.6 References

8-1 G. Battistoni, A. Ferrari and P. R. Sala, Background calculations for the ATLAS detector and hall, ATLAS Internal Note GEN–NO–10; A. Ferrari and P. R. Sala, ATLAS Internal Note MUON–NO–90.

8-2 R. Cardarelli, A. Di Ciaccio and R. Santonico, Performance of a resistive plate chamber operating with pure CF_3Br, Nucl. Instrum. Methods A 333 (1993) 399.

8-3 R. Cardarelli, V. Makeev and R. Santonico, Avalanche and streamer mode operation of resistive plate chambers, Nucl. Instrum. Methods A 382 (1996) 470.

8-4 R. Santonico, Topics in resistive plate chambers, in Proceedings of the 3rd International Workshop on Resistive plate Chambers and Related Detectors, Pavia 11–12 October 1995 (eds. S. Ratti and M. Merlo).

8-5 M. Atac et al., Nucl. Instrum. Methods A 300 (1982) 345.

8-6 M. Abbrescia et al., Resistive plate chambers working at high rate, Nucl. Phys. B (Proc. Suppl.) 44 (1995) 218.

8-7 M. Angelone et al., Test of a resistive plate chamber under irradiation of photons and neutrons, Nucl. Instrum. Methods A 355 (1995) 399.

8-8 V. Ammosov et al., ATLAS Internal Note MUON–NO–082.

8-9 R. de Asmundis et al., Performances of the RPC trigger system in the L3 experiment, Proceedings of the 3rd International Workshop on Resistive plate Chambers and Related Detectors, Pavia 11–12 October 1995 (eds. S. Ratti and M. Merlo); G. Carlino et al., RPC performances at L3 experiment, L3 internal note no. 1811.

8-10 The BaBar Collaboration, Technical Design Report (March 1995).

8-11 R. Cardarelli, Gli RPC come rivelatore di trigger muonico a LHC, Invited Talk at LXXXII Congresso Nazionale Societa' Italiana di Fisica, Verona, 23–28 September 1996.

8-12 A. Longoni et al., Some considerations about the use of HEMTs in preamplifiers for radiation detectors, Proceedings of the IV Meeting di Elettronica Integrata per la Fisica delle Alte Energie, Isola del Giglio 28–30 / 5 / 1993.

8-13 C. Bacci et al., The first-level muon trigger in the central toroid of the ATLAS experiment, Nucl. Instrum. Methods A 367 (1995) 428.

8-14 C. Bacci et al., Test of a resistive plate chamber operating with low gas amplification at high intensity beams, Nucl. Instrum. Methods A 352 (1995) 552.

8-15 A. Di Ciaccio et al., Test of low gas gain RPCs with ozone and non ozone depleting gas mixtures, Proceedings of the 3rd International Workshop on Resistive plate Chambers and Related Detectors, Pavia 11–12 October 1995 (eds. S. Ratti and M. Merlo).

8-16 M. Della Negra et al., Study of muon triggers and momentum reconstruction in a strong magnetic field for a muon detector at LHC, CERN / DRDC / 90–36, DRDC / P7.

8-17 M. G. Alviggi et al., Resistive plate chambers in ATLAS, ATLAS Note MUON–NO–131, Nucl. Instrum. Methods A 384 (1996) 222.

8-18 C. Nuttall; private communication.

8-19 S. Veneziano et al., A test of the ATLAS first level muon trigger logic, Proceedings of the 3rd International Workshop on Resistive plate Chambers and Related Detectors, Pavia 11–12 October 1995 (eds. S. Ratti and M. Merlo).